

Emergence of hairpins in the conformations of a confined polymer

E. Werner¹, A. Jain², A. Muralidhar², K. Frykholm³, T. St Clere Smithe¹, J. Fritzsche⁴, F. Westerlund³, K. D. Dorfman², B. Mehlig¹

¹*Department of Physics, University of Gothenburg, Origovägen 6B, 412 96 Göteborg, Sweden*

²*Department of Chemical Engineering and Materials Science, University of Minnesota – Twin Cities, 421 Washington Avenue SE, Minneapolis, Minnesota 55455, USA*

³*Department of Biology and Biological Engineering,*

Chalmers University of Technology, Kemivägen 10, 412 96 Göteborg, Sweden and

⁴*Department of Physics, Chalmers University of Technology, Kemigården 1, 412 96 Göteborg, Sweden*

If a semiflexible polymer confined to a narrow channel bends around by 180 degrees, the polymer is said to exhibit a hairpin. The equilibrium extension statistics in either the limit where hairpins are rare or in the limit where they are common have been characterized in detail. In this article we consider the intermediate situation, where hairpins are rare but common enough to influence the extension statistics. We study the equilibrium distribution of the extension, as well as the approach to equilibrium, by a combination of theoretical analysis, Monte Carlo simulations, and experiments on DNA coated by the protein RecA, which enhances the stiffness of DNA by approximately one order of magnitude. We find good agreement between the model and simulations. The model also provides excellent agreement with experimental data provided that we assume a persistence length of 2 μm for the RecA-DNA filament.

I. INTRODUCTION

A semiflexible polymer confined to a very narrow channel is almost perfectly extended and aligned with the channel axis. Small deviations from perfect alignment yield an extension slightly smaller than the contour length of the polymer [1]. In this so-called Odijk regime, the equilibrium statistics of the polymer extension approach a Gaussian distribution in the limit of large contour length. The mean and variance of this distribution are known to high precision [2]. For a wormlike chain with persistence length ℓ_P confined to a rectangular channel with largest side length D_W , this regime is obtained when $D_W \ll \ell_P$ [3–5].

For larger channel widths ($D_W \approx \ell_P$), the polymer can turn around in the channel forming a so-called ‘hairpin’. This is illustrated in Fig. 1. As a result, the conformational statistics depend on the interaction between hairpin segments. In this paper we consider self-avoiding polymers with the strength of the interaction parametrized by the polymer width, w . The limit $w = 0$ corresponds to an ideal polymer where self-avoidance does not matter. In this case the typical length of a hairpin defines a length scale g , known as the global persistence length [3, 6]. If the contour length L is much larger than g then there are multiple hairpins in any channel segment, and the distribution of the extension approaches that of a one-dimensional random walk of $\approx L/g$ steps of length $\approx g$ [3, 4].

What happens when w is not zero? The importance of the parameter w is quantified by Odijk’s scaling parameter

$$\xi = \frac{gw}{D_H D_W^{2/3} \ell_P^{1/3}}, \quad (1)$$

where the channel height D_H is assumed to be smaller than the channel width, $D_H \leq D_W$. This parameter

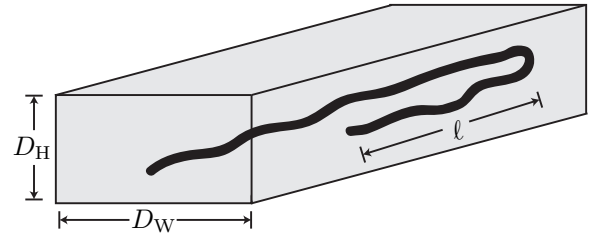


FIG. 1. Schematic of a confined wormlike chain confined in a channel of width D_W and height $D_H < D_W$, showing a configuration with a single hairpin of length l .

measures the expected number of overlapping points between the two strands of a hairpin of length g [3–5]. The effect of self-avoidance depends on the magnitude of ξ . If $\xi \gg 1$, hairpins are rarely observed, as it would be very difficult for the two strands of a hairpin to avoid overlapping with each other. As a result, in this regime the configuration statistics are in approximate agreement with the predictions of the Odijk regime [3, 4]. If on the other hand $\xi \ll 1$, then self-avoidance has a negligible effect on the likelihood of forming a hairpin. Yet for a long polymer the effect on macroscopic observables such as the extension can be very significant. For example, while the average extension of a long ideal polymer ($w = 0$) grows as $\langle X \rangle \sim \sqrt{L}$, for a self-avoiding polymer the scaling of the extension is always linear in L in the limit $L \rightarrow \infty$, no matter how small $w > 0$.

The results summarized above apply provided that $L \gg g$. However, since the global persistence length g increases without bound when the channel size decreases [4, 6], the inequality $L > g$ can be violated even for very long polymers.

In this article we therefore investigate the conformational statistics of a polymer with $L < g$. We measure in

simulations the equilibrium distribution of the extension and show that the shape of this distribution can be explained by a theory that relies on a series expansion. The simulation results are explained by keeping only the first two terms in this expansion, corresponding to conformations with no or one hairpin. This reflects the rarity of hairpins but their substantial impact nonetheless on the extension statistics.

We compare simulations and theory against experiments using DNA covered with the protein RecA. The DNA-RecA complex is a polymer with a persistence length that is an order of magnitude larger than that of bare DNA. This means that the polymer physics of interest can be visualized in much larger channels (600 nm–3 μ m) where the resolution is not limited by light diffraction. This has two consequences. First, it allows us to visualize the underlying configurations akin to previous experiments using fluorescent actin filaments [7]. Second, in the wider channels the extension of the confined molecules is dominated by hairpin configurations (Fig. 1). We find good agreement between theory, simulations and experiments assuming that the persistence length of RecA-coated DNA is approximately $\ell_P = 2 \mu$ m. We note that this value is considerably larger than most previous measurements reported in the literature.

Our experimental system also furnishes an opportunity for studying the dynamics of confined polymers. Analyzing the subset of molecules which are free of hairpins, we find good qualitative agreement with existing theories for the dynamics in the Odijk regime [8–10]. Since these theories have previously only been tested against bare DNA, this is a powerful test of their general validity. We further discuss how the dynamics are affected by the emergence of hairpins. We show that the hairpin dynamics are stochastic. This behavior contrasts with previous work on unfolding of bare DNA in channels [11, 12], where the unfolding dynamics are captured by a deterministic model that balances friction with the deterministic entropic force arising from excluded volume [11].

II. METHODS

A. Simulations

Our equilibrium simulations use a discretized worm-like chain model [13]. The discretization is made using a touching-bead model, with $N + 1$ beads of diameter w connected by rigid bonds. A bending potential determines the stiffness of the chain:

$$U(\theta_1, \dots, \theta_N) = k_B T \kappa \sum_{n=1}^{N-1} (1 - \cos \theta_n). \quad (2)$$

The index n ranges over bonds, θ_n is the angle between bonds n and $n + 1$, and κ is known as the ‘bending constant’. The persistence length in this model is defined

as

$$\ell_P = w \sum_{k=0}^{\infty} \langle \mathbf{t}_n \mathbf{t}_{n+k} \rangle \quad (3)$$

where \mathbf{t}_n is the tangent vector to the chain at bond n , and the average should be computed for an ideal and unconfined chain. The persistence length can be expressed in terms of κ and w [14]:

$$\frac{\ell_P}{w} = \frac{\kappa}{\kappa - \kappa \coth \kappa + 1} \approx \kappa. \quad (4)$$

The channel extends in the x -direction. Excluded volume interactions are incorporated into the model by imposing an infinite energy barrier for bead-bead overlap and bead-wall overlap.

We simulate this model using the pruned-enriched Rosenbluth method (PERM) [15, 16], following the approach described in our previous work in this area [14, 17]. PERM is a biased chain growth method that provides, *inter alia*, information on the extension statistics while avoiding the attrition problem in self-avoiding random walks. The PERM simulations were conducted to grow chains up to 1501 beads using the parameters appearing in Table I. Distributions of the mean span were obtained from 2×10^6 tours, corresponding to 1.7×10^7 configurations.

In previous work, we generally computed expectation values on-the-fly during the chain growth. In the present contribution, we modified our program to compute histograms for the probability $\rho(X)$ of observing a particular value of the extension X . We also added functionality that outputs configurations and their corresponding statistical weights for post-processing. The configuration of a polymer chain allows us to calculate the hairpin contour lengths as a post-processing step. For the latter analysis, we consider a moving window of 50 beads and compute the span and end-to-end distance for the sub-chain corresponding to each window. If these two sizes are equal, then there is no hairpin within the window; otherwise, the window is flagged as a hairpin. Typically, a given hairpin will involve multiple contiguous windows, which are grouped into a single hairpin event by a clustering algorithm. Within each cluster, we then identify the bead with the minimum value of $|x_i|$ and assign the hairpin location to that bead. If the algorithm identifies two or more hairpin strands, and we use the shortest strand length as ℓ provided that its span in the channel is larger than 1 μ m. We found that this binning and clustering method is necessary because the simulations have much higher spatial resolution (equal to w) than the corresponding experiments; a bead-by-bead analysis leads to many very small hairpins that do not correspond to the global hairpins that are relevant in experiments.

To determine the global persistence length, we follow an existing approach for rectangular channels [18] which we describe in detail in the supplemental material.

L	ℓ_P	w	D_H	D_W
15 μm	2 μm	10 nm	140 nm	0.6, 0.9, 1.3, 1.8, 2.4, 3.0 μm

TABLE I. Parameters used in the simulations and theoretical description of the RecA-DNA complex. The contour length used in the simulations is a representative value for the RecA-DNA filaments observed in experiments such as those in Fig. 1. The value of the persistence length was selected by comparison between simulation data and experiment. The value of the effective width represents an approximation for the thickening of naked DNA from coating with RecA.

B. Experimental details

Our experiments used a nanofluidic device, fabricated as described in Ref. [19]. The nanochannel width ranged from 600 nm to 3000 nm (see Table I). The channels were passivated using a lipid bilayer as previously described [20]. Double-stranded DNA, either λ -DNA (New England Biolabs) or T4-DNA (Wako Chemicals), was coated with fluorescently labeled RecA protein as described in Ref. [19]. The resulting RecA-DNA filaments were conducted from a channel of one width to a channel of another width using pressure-driven flow. In this way, we could observe the same RecA-DNA filament at different values of D_W and could study how the filament conformations depend upon D_W . After moving the filament into a given channel position, microscope recordings of the filament were made while uniform pressure was maintained in the nanochannel. The fluorescence microscopy set-up was a Zeiss Axiovision microscope equipped with a 100 W mercury lamp, a Photometrics Evolve EMCCD camera, and a 100 \times oil immersion TIRF objective (NA = 1.46) from Zeiss. One video of 400 frames was recorded for each channel width, for each filament. The time interval between frames was 0.11 seconds. The contour lengths of the T4-DNA complexes ranged from 7 microns to 21 microns, and those of the λ -DNA complexes ranged from 11 microns to 23 microns. One experimental uncertainty is that since only the protein fluoresces, DNA that is not coated by RecA is invisible in our experiments. It is therefore possible that such invisible DNA is attached at one or both ends of the visible filament. This could have a small effect on the equilibrium statistics, as excluded volume interactions between the bare and coated DNA could reduce the probability of observing hairpins. More importantly, hydrodynamic friction between the bare DNA and the surrounding solution might slow down the dynamics.

C. Image analysis

Kymographs were produced by stacking into a column the intensity profiles (defined below) produced for each sequence of frames, so that each row of the column represents

a single frame of the experimental recording. To produce the intensity profiles, the section of the frame containing the molecule was identified by locating the region with the maximal brightness. Next, the pixel intensity was averaged over the direction perpendicular to the channel, resulting in a row of pixel values which we interpret as the intensity profile along the channel. Kymographic representations of all experimental videos are included in the supplemental material [21].

To extract the extension as a function of time, we fit the brightness value at each row of the kymograph to an error function ‘box’ curve described by $\alpha + \beta(\text{erf}[\gamma(x - x_0)] - \text{erf}[\varepsilon(x - x_1)])$, where x is the location along the channel [22]. In practice, we found that we could obtain somewhat more robust results for the extension by modifying the algorithm for computing the kymographs. Instead of creating the intensity profile by averaging across the channel, we first smoothed each video frame by a median filter of radius 2 pixels, and defined the profile as the maximum pixel intensity in each column. Further, before fitting to the box curve described above, we smoothed the resulting kymograph by a moving time average with a window size of 3 frames and a moving space average of window size 4 pixels.

III. EQUILIBRIUM DISTRIBUTION

A. Theory

In this article we analyse the conformations of polymers that are shorter than the global persistence length, $L < g$. As mentioned in the introduction, such polymers may sometimes exhibit hairpin-configurations, and sometimes not. Since the mechanisms determining the polymer extension X are quite different if hairpins are present or absent, it is necessary to consider these possible configurations separately, before combining them into a single distribution $\rho(X)$:

$$\rho(X) = \sum_{j=0}^{\infty} \rho_j(X) P_j. \quad (5)$$

Here, $\rho_j(X) \equiv \rho(X|N_h = j)$ is the distribution of X conditional on that the number N_h of hairpins equals j , and $P_j \equiv \text{prob}(N_h = j)$ is the probability of observing j hairpins. Since this article is concerned with the situation where hairpins are rare, we restrict the following discussion to the two cases of either zero or one hairpins.

We first consider the distribution $\rho_0(X)$ for a polymer without hairpins. When $L \gg \lambda \approx D_W^{2/3} \ell_P^{1/3}$ the distribution is Gaussian

$$\rho_0(x) = (2\pi\sigma_{\text{Od}}^2)^{-1/2} \exp\left[-\frac{(X - \mu_{\text{Od}})^2}{2\sigma_{\text{Od}}^2}\right] \quad (6)$$

with mean and variance which to a good approximation

is given by the statistics of the Odijk regime [2],

$$\mu_{\text{Od}} = L \left(1 - 0.091 \frac{D_{\text{H}}^{2/3} + D_{\text{W}}^{2/3}}{\ell_{\text{P}}^{2/3}} \right), \quad (7)$$

$$\sigma_{\text{Od}}^2 = 0.0048L \left(\frac{D_{\text{H}}^2 + D_{\text{W}}^2}{\ell_{\text{P}}} \right). \quad (8)$$

We turn now to the case of one hairpin. Let ℓ denote the length of the shortest hairpin strand, as illustrated in Fig. 1. In this configuration, the extension is, to a good approximation, given by the extension of the longest hairpin strand, which obeys Odijk statistics with a contour length of $L - \ell$. For ideal polymers, i.e. without interactions between the two strands of the hairpin, the hairpin length is drawn uniformly between 0 and $L/2$. Thus

$$\begin{aligned} \rho_1^{\text{id}}(X) &\approx \frac{2}{L} \int_0^{L/2} d\ell \rho_0(X; L - \ell) \\ &\approx \frac{1}{\mu_{\text{Od}}} \left[\text{erf} \left(\frac{2X - \mu_{\text{Od}}}{2\sigma_{\text{Od}}} \right) - \text{erf} \left(\frac{X - \mu_{\text{Od}}}{\sqrt{2}\sigma_{\text{Od}}} \right) \right] \end{aligned} \quad (9)$$

Here, $\rho_0(X; L)$ is the extension distribution in Eq. (6) of a polymer segment of length L that is free of hairpins.

We then need to modify Eq. (9) to account for excluded volume. If the polymer is self-avoiding then configurations with large ℓ are penalized. The probability of overlaps between these two strands can be estimated by a mean-field argument [3, 18], yielding

$$P_{\text{no overlap}}(\ell) = \exp(-\alpha\xi\ell/g) \quad (10)$$

where α is a prefactor of order unity. For future reference, it proves convenient to define the length scale

$$\ell_{\text{SA}} \equiv \frac{g}{\alpha\xi} \quad (11)$$

such that

$$P_{\text{no overlap}}(\ell) = \exp(-\ell/\ell_{\text{SA}}). \quad (12)$$

This overlap length-scale quantifies the hairpin length at which self-avoidance becomes important.

Eqs. (10)–(12) allow us to compute how to modify Eq. (9) in the presence of self-avoidance. The integrand in Eq. (9) must include an extra factor proportional to $(1 - P_{\text{no overlap}}(\ell))$. Performing the integration yields

$$\begin{aligned} \rho_1(X) &\propto \\ &\left[\text{erf} \left(\frac{2X - \mu_{\text{Od}}}{2\sigma_{\text{Od}}} \right) - \text{erf} \left(\frac{X - \mu_{\text{Od}}}{\sqrt{2}\sigma_{\text{Od}}} \right) \right] \exp \left(\frac{X - L/2}{\ell_{\text{SA}}} \right), \end{aligned} \quad (13)$$

where, for the sake of brevity, the normalizing prefactor is not shown.

To determine the first two terms in Eq. (5) we also require P_0 and P_1 . For ideal polymers, the formation of a hairpin bend at a given location is independent of how many other hairpins have already formed. It follows that the number of hairpins is Poisson distributed, with

a rate constant $\mu \propto L/g$. A precise calculation yields $\mu = L/(2g)$. It follows that $P_1^{\text{id}}/P_0^{\text{id}} = L/(2g)$. We also note that $P_2^{\text{id}}/P_0^{\text{id}} = L^2/(8g^2)$, so the contribution of two hairpins to $\rho(X)$ is small when $L \ll g$.

Now consider a self-avoiding polymer. It is less likely than an ideal polymer to exhibit hairpins, as only a fraction of all ideal configurations with a hairpin are free of overlaps. We denote this fraction by

$$\begin{aligned} \langle P_{\text{no overlap}} \rangle &\equiv \frac{2}{L} \int_0^{L/2} P_{\text{no overlap}}(\ell) d\ell \\ &= \frac{2\ell_{\text{SA}}}{L} \left[1 - \exp \left(-\frac{L}{2\ell_{\text{SA}}} \right) \right]. \end{aligned} \quad (14)$$

This implies that

$$\frac{P_1}{P_0} = \frac{L}{2g} \langle P_{\text{no overlap}} \rangle = \frac{\ell_{\text{SA}}}{g} \left[1 - \exp \left(-\frac{L}{2\ell_{\text{SA}}} \right) \right]. \quad (15)$$

As expected, the limit $\ell_{\text{SA}} \gg L$ reproduces the ideal result. The opposite limit yields a ratio that is independent of L . In summary, Eqs. (5), (6), (13), and (15) yield the desired approximation for the distribution $\rho(X)$ of the extension X .

B. Simulations

In order to compare the theoretical predictions against numerical simulations, we first need to determine the global persistence length. Odijk [3, 6] proposed a mechanical theory for computing the global persistence length. However, recent simulations of confined worm-like chains have suggested that the Odijk theory overestimates the global persistence length [4, 18, 23]. While the functional form of Odijk's theory appears to be reasonable for square and circular channels [4, 23], requiring only an additional channel-size-independent energetic contribution to bring the theory in line with simulations, even the functional form of the theory seems to differ from simulation data for rectangular channels [18]. Therefore we decided to determine the values of g for our particular channels via simulation.

Table II presents the values of g obtained from simulations (see supplemental material [21]). For channels with $D_{\text{W}} = 900$ nm and larger, we could reliably extract a value of the global persistence length. For the smallest channel, we were not able to compute a value of g from the simulations [21]. This suggests that g is larger than the maximal contour length that we could simulate. In principle, this limitation can be surmounted by increasing the contour length of the simulated ideal chains. In practice, we expect that g increases exponentially with decreasing $D_{\text{W}}/\ell_{\text{P}}$ [6]. As a result, the requisite contour length quickly becomes infeasible to simulate, even using a biased-growth method like PERM. In what follows, we simply set $g = \infty$ for the smaller channels.

The second key parameter we must extract from the simulations is the self-avoidance length scale ℓ_{SA} or,

D_W (μm)	0.6	0.9	1.3	1.8	2.4	3.0
g (μm)	—	13000	350	90	37	22
ξ	—	780	17	3.5	1.2	0.61
ℓ_{SA} (μm)	—	9.4	12	15	18	21

TABLE II. Summary of simulation data and corresponding theory parameters. The values of g are obtained from simulations of ideal chains for the parameters in Table I (see supplemental material [21]). The — entries indicate channel sizes where g could not be measured. The values of the scaling parameter ξ are computed from Eq. (1). The values of the self avoidance length scale ℓ_{SA} are obtained from Eq. (11) using the value of α computed from Fig. 2.

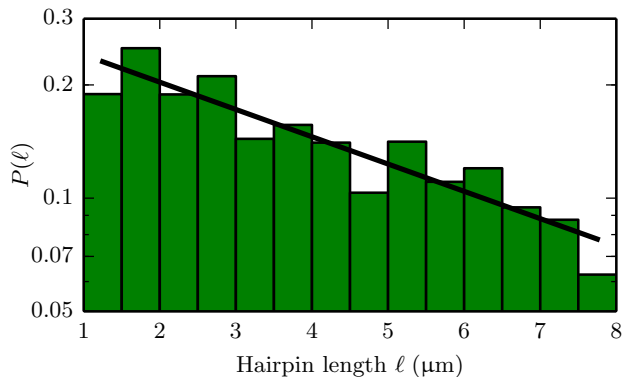


FIG. 2. Semi-logarithmic plot of the probability distribution of the hairpin length for a polymer with persistence length $\ell_P = 1150$ nm, in a channel of width $D_W = 600$ nm. The solid line indicates an exponential fit to the distribution, leading to $\ell_{\text{SA}} = 6.0$ μm . Together with simulated values for g and ξ (see supplemental material [21]), this gives us a dimensionless prefactor of $\alpha = 1.7$ after comparing against Eq. (10).

equivalently, the prefactor α in Eq. (10). Figure 2 shows the probability distribution of hairpin lengths for a self-avoiding polymer in a channel. For these simulations, we used a polymer with a persistence length of $\ell_P = 1150$ nm confined to a channel of width $D_W = 600$ nm. The value of ℓ_{SA} is obtained by fitting the distribution to Eq. (12); as seen in Fig. 2. The parameter α must be independent of the channel size. We thus used the result from Fig. 2 to compute values of ℓ_{SA} in Table II. To compute this data, we used 3×10^5 tours, corresponding to 2.7×10^6 configurations.

Having determined the prefactor α and the values of g for each channel size, we can now compare theory against simulations for the distribution of X/L , without any fitting parameters. The result is shown in Fig. 3. We find excellent agreement for the narrower channels. For larger channels the theory underestimates the width of the peak at large extension, as well as its skewness. This is a result of the assumption that Odijk theory [Eqs. (7)–(8)] describes the statistics of each hairpin, but this assump-

tion starts to fail when $D_W \approx \ell_P$.

C. Comparison with experiment

Figure 4 compares the distribution of the extension that we measure in experiments against the results from simulations. Since it is hard to determine the experimental contour length precisely enough, we normalize the polymer extension by the median polymer extension in the narrowest channel rather than the contour length. (Note that this procedure only allows us to analyze the subset of molecules which have been imaged in the narrowest channel). Further, in order to compare simulations against experiments, we must determine the value of ℓ_P that best describes the RecA-DNA-complex. To this end, we measure the median extension for each channel size, and compare the results against simulations for different values of ℓ_P . The results are shown in Fig. 5. We find the best fit between simulations and experiment when ℓ_P is close to $2 \mu\text{m}$. We have therefore used the value $\ell_P = 2 \mu\text{m}$ in Fig. 4, as well as in the rest of the simulations that we report on in this paper. We note, however, that the value found here for the persistence length is significantly higher than the values reported for the RecA-complex in Refs. [19, 24]. At present we do not know the reason for this discrepancy. But we emphasize that $\ell_P = 2 \mu\text{m}$ not only gives excellent agreement for the median of the polymer extension, this value also yields good agreement between experiments and simulations for the entire shape of the distribution (Fig. 4).

IV. DYNAMICS

As is the case for the equilibrium statistics, the conformational dynamics are very different depending on whether there are hairpins or not. We therefore consider the two cases separately.

A. Relaxation time for configurations without hairpins

A simple description of the dynamics of the extension in the hairpin-free state is offered by comparing the system to a particle diffusing in a harmonic potential [8–10]. If the instantaneous extension deviates from the mean extension then the polymer experiences a restoring force $F = -k(X - \mu_{\text{Od}})$, where $k = k_B T / \sigma_{\text{Od}}^2$. In addition, as the extension changes the segments of the polymer move through the water, leading to a friction force $F \approx -\zeta \dot{X}$. The friction coefficient ζ is defined in the following way: Imagine that the polymer is dragged slowly along the channel with a velocity v . The opposing force acting on the polymer is then proportional to v , with proportionality constant ζ . Since a change in the polymer extension requires that a large fraction of the polymer segments

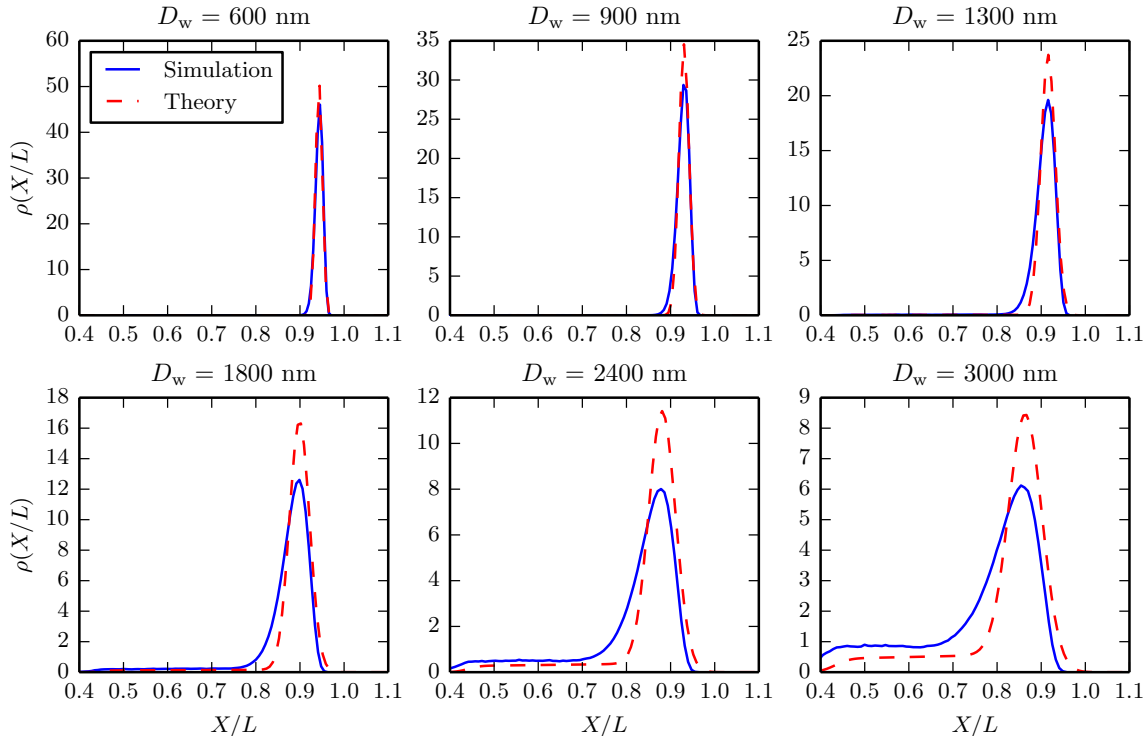


FIG. 3. Comparison of distributions obtained from simulations (section III B) against theory (section III A), for the parameter values $L = 15 \mu\text{m}$ and $\ell_p = 2 \mu\text{m}$. For the narrowest channel we assume $g = \infty$ in the theory, i.e. no hairpins.

move, we can assume that $v \approx \dot{X}$. It follows that a change in the extension leads to an average friction force $F \approx -\zeta \dot{X}$. The two parameters k and ζ give rise to a relaxation time $\tau_{\text{relax}} \approx \zeta/k \approx \zeta \sigma_{\text{Od}}^2 / (k_B T)$. Following the notation of [10] we obtain the prediction

$$\tau_{\text{relax}} = c \frac{\sigma_{\text{Od}}^2}{2k_B T} \zeta, \quad (16)$$

where c is a dimensionless factor of order unity.

Since ζ is not known for rectangular channels, we use the value for a square channel of size D_H (the smaller dimension). Applying the results of Ref. [25] yields

$$\zeta = \frac{7.7\eta L}{\log(D_H/d)}, \quad (17)$$

where $d \approx 10 \text{ nm}$ is the hydrodynamic diameter of the polymer and η is the viscosity of the solution. Because of the logarithmic dependence, ζ is relatively insensitive to changes in either D_H or d .

To analyze the dynamics in the hairpin-free state, we determine by inspection which of the experimental videos are free of hairpins, and analyze their dynamics separately. We determine the experimental relaxation time by measuring the autocorrelation function

$$C(\tau) = \frac{\langle [X(t) - \langle X \rangle][X(t+\tau) - \langle X \rangle] \rangle}{\langle [X(t) - \langle X \rangle]^2 \rangle}, \quad (18)$$

as shown in the supplemental material [21]. From these experimental measurements we estimate the autocorrelation time in two ways, either by fitting an exponential function at short times, or by integrating the autocorrelation function from zero up to a cutoff (see supplemental material [21]). The resulting estimates are shown in Fig. 6.

The experimental estimates in Fig. 6 are also compared against Eq. (16). We see that the measured time scale is in qualitative agreement with Eq. (16). Since previous tests of this theory were performed on bare DNA, whose persistence length differs by more than an order of magnitude from the molecule we study, this is a strong confirmation of the theory. It must be noted, however, that we do not know whether invisible, bare DNA is attached to the ends of the polymer (see section II B). Such attached DNA would tend to increase the relaxation time, but is not considered in our theoretical description.

B. Diffusion model for hairpin size

A hairpin configuration can be modeled as two polymer strands, connected at one end. If one of the strands is much longer than the other it is practically immobile. The shorter strand diffuses like a polymer in the Odijk regime, with diffusion constant $k_B T / \zeta(\ell)$ [25]. The

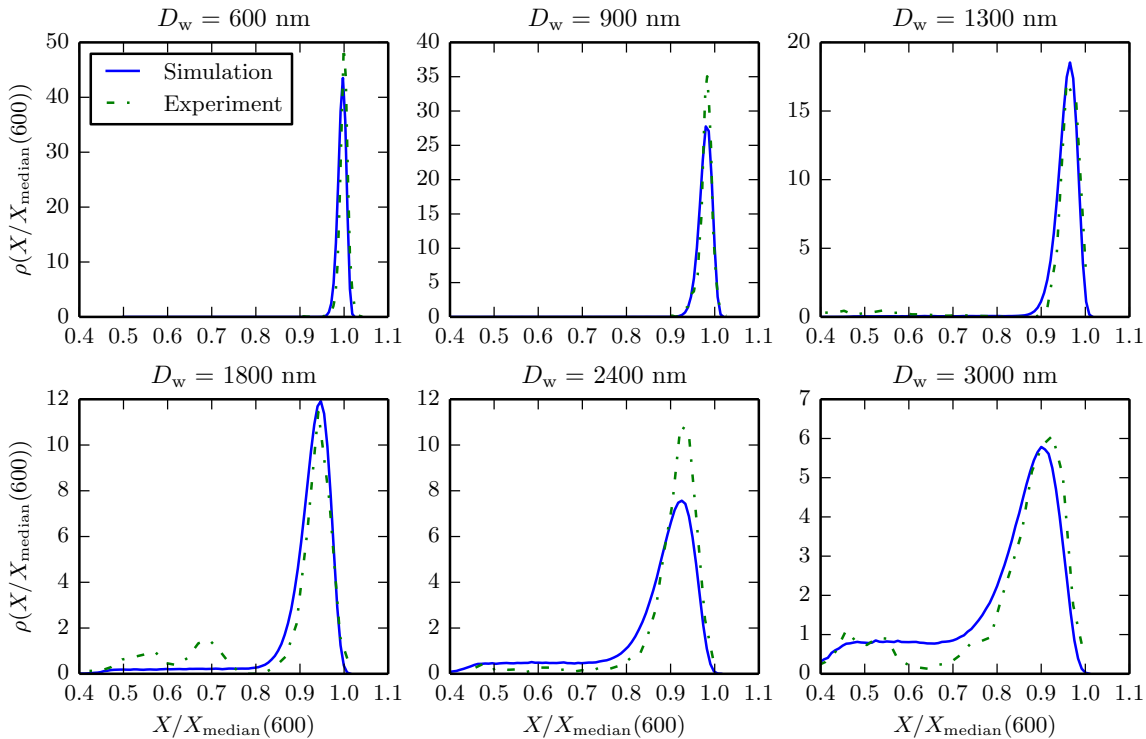


FIG. 4. $P(X)$ from computer simulations and experiments. Simulation parameters as in Fig. 3. Since we cannot measure the contour length to sufficient accuracy in experiments, we instead normalize X by dividing the extension with the median extension in the narrowest channel, a proxy for the contour length. The experimental data consist of the subset of experiments for which the same molecule was measured both in the channel under consideration and in the narrowest channel, and further where the median extension in the narrowest channel agrees to within 20% with the value found in simulation. Further, we removed two molecules that exhibited a hairpin in the narrowest channel, in which case the median extension is not a good proxy for the contour length.

length of the hairpin changes as it diffuses. In addition to the diffusive motion, the strand experiences an unfolding force f , due to the collisions between the two strands. This force is discussed below. The simultaneous action of diffusion and the constant unfolding force can be described by a generalized diffusion equation,

$$\frac{\partial \rho(\ell)}{\partial t} = -\frac{\partial}{\partial \ell} \left[\frac{f}{2\zeta(\ell)} \rho(\ell) \right] + kT \frac{\partial}{\partial \ell} \left[\frac{1}{2\zeta(\ell)} \frac{\partial}{\partial \ell} \rho(\ell) \right]. \quad (19)$$

Note that this equation has the equilibrium distribution $\rho_{\text{eq}}(\ell) \propto \exp[\int^\ell f/(k_B T) d\ell']$, in agreement with the Boltzmann distribution if the force is given by the derivative of an energy as $f = -\partial E/\partial \ell$. Further, in the deterministic limit, i.e. where the last term is negligible, Eq. (19) is consistent with the deterministic description of an unfolding process given in Refs. [11, 26], as well as with the description of ejection of a polymer out of a nanochannel [27].

The force f in Eq. (19) is due to the self-avoiding interaction between the two strands in the folded configuration that tends to unfold the hairpin. This can be modeled by an entropic force given as the slope of the

free energy [28]. Eq. (10) shows that this force is:

$$\begin{aligned} f &= k_B T \frac{\partial \log P_{\text{no overlap}}}{\partial \ell} = \frac{-k_B T}{\ell_{\text{SA}}} \\ &= -\alpha k_B T \frac{w}{D_H \ell_P^{1/3} D_W^{2/3}}. \end{aligned} \quad (20)$$

Eq. (19) allows one to define two timescales for a hairpin of length ℓ , one diffusive time scale $\tau_{\text{diff}} = \zeta(\ell)\ell^2/(kT)$ and one deterministic time scale $\tau_{\text{drift}} = \zeta(\ell)\ell/f$. In drift-diffusion problems, the relative effects of drift to diffusion is captured by the ratio of these time-scales, namely the Péclet number $\text{Pe} = f\ell/kT$. For a hairpin of length $3 \mu\text{m}$ in a 1300 nm channel, we find $\text{Pe} \approx 0.2$, suggesting that drift is a small effect. The prediction that the unfolding dynamics of a RecA-DNA hairpin are diffusive contrasts with the predominantly deterministic dynamics seen in experiments on bare DNA [11, 12]. This prediction is validated by the experimental data shown in Fig. 7. The Figure shows an example where the hairpin length first shrinks and then grows, demonstrating that the dynamics are far from deterministic. Since only a small fraction of our experiments show hairpins we do not have enough data for a quantitative test of Eq. (19).

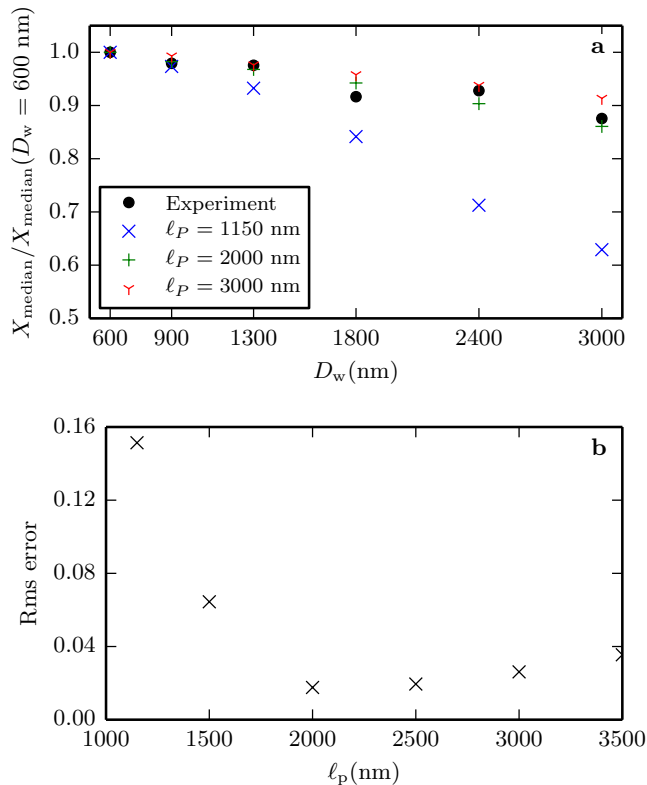


FIG. 5. Comparison of simulations against experiments, to establish which value of ℓ_P fits best. **a**. Comparison of the median extension from experiments against simulations for different values of ℓ_P . The median extension is normalized by the value measured in the narrowest channel (as in Fig. 4). **b**. The root-mean squared (rms) difference between the simulated value and the experimental value shown in panel **a**, averaged over all channels except the smallest (where the difference is zero by construction).

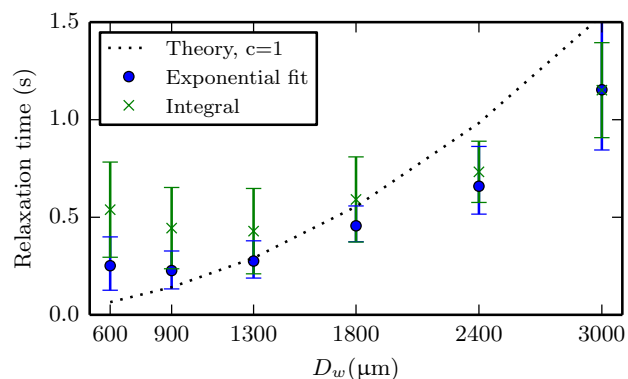


FIG. 6. Experimental estimates of the relaxation time of hairpin-free polymers (see supplemental material [21]), compared against Eq. (16). The experimental estimates were obtained by integrating the average autocorrelation in each channel for 20 frames (crosses), and by fitting the exponential falloff for the first 4 frames (circles). The vertical bars indicate the variability between molecules, see supplemental material [21].

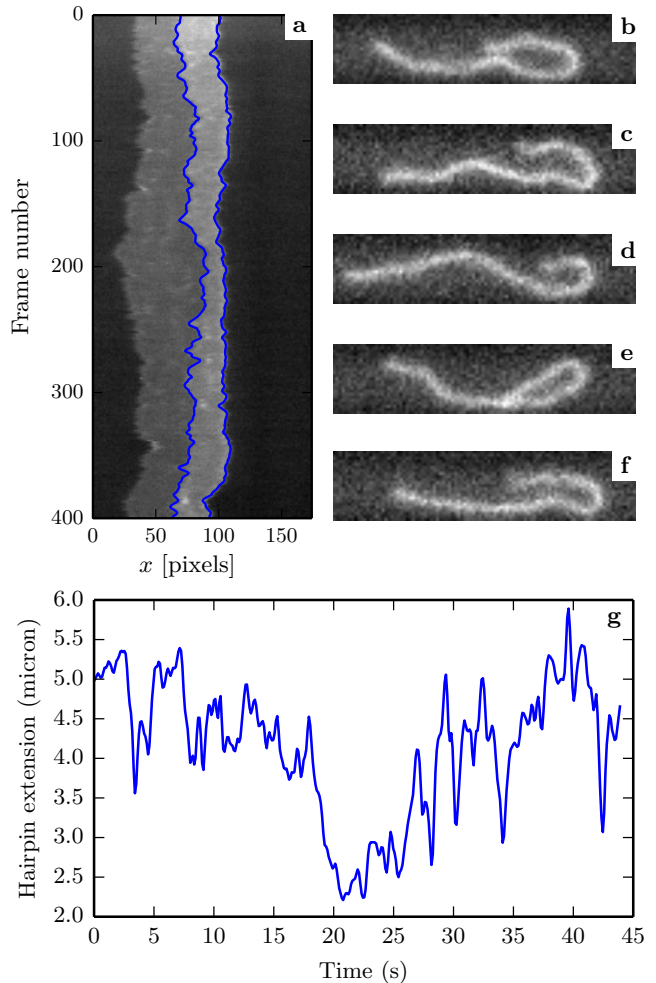


FIG. 7. **a** Kymograph, λ -DNA, channel width $D_w = 2.4 \mu\text{m}$. Blue lines indicate the edges of the hairpin, as identified by the algorithm described in Section II C. Panels **b** to **f** show cropped microscope images of the confined molecule (frame numbers 1, 100, 200, 300 and 350). Panel **g** shows the extension of the hairpin as a function of time. Note that the extension decreases significantly before increasing again, showing that the hairpin extension dynamics are non-deterministic.

V. CONCLUSIONS

In this article we investigated the probability of hairpin formation for a wormlike chain under strong channel confinement, and calculated the effect of hairpins on the equilibrium distribution and the relaxation dynamics of the extension.

In the limit where self-avoidance is negligible (ideal chain), we found that the probability of hairpin formation is determined by the ratio g/L of two length scales: the global persistence length g [3, 4] and the contour length L of the polymer. The number of hairpins is Poisson distributed with mean $L/(2g)$.

When self-avoidance cannot be neglected, a third

length scale appears: ℓ_{SA} , the hairpin length at which the expected number of overlaps between the two strands of the hairpin equals unity. When $g \gg L$ hairpins are rare. In this limit we derived an equation for the probability of observing a hairpin in terms of L , g , and ℓ_{SA} . Building on known results for the distribution of the extension in the Odijk regime [2], we derived an expression for the distribution that includes also the effect of a single hairpin.

We tested these results against Monte-Carlo simulations of a discrete wormlike chain model, as well as against experimental measurements on RecA-coated DNA confined to rectangular nanochannels. In contrast with bare DNA, the persistence length of this DNA-protein complex is larger than the wavelength of light, thereby allowing the visualization of microscopic conformations. The experimental measurements only match with simulations and theory if the RecA-DNA complex is assumed to have a persistence length of $\approx 2 \mu\text{m}$ (see section III C). This value is larger than that found in most other studies. However, one previous study [29] found a persistence length of $2.1 \pm 0.1 \mu\text{m}$ for single-stranded DNA covered with RecA, albeit under experimental conditions that differ from ours in some aspects. Since not much is known about what determines the persistence length of the RecA-DNA complex, we do not know the reason for the discrepancy between different measurements.

Our experimental system makes it possible to study the dynamics of a confined polymer in a new setting. For configurations without a hairpin, our experiments are in good qualitative agreement with theoretical models for the Odijk regime [10]. Previously, these models had been compared against experimental results obtained for

uncoated, bare DNA [9]. Since the persistence length of RecA-coated DNA differs from that of bare DNA by more than an order of magnitude, our experimental results provide a strong test of this theory.

Whereas the dynamics of hairpin-free polymers seem to be consistent between bare DNA and RecA-DNA, the hairpin dynamics of RecA-DNA are very different than the corresponding dynamics of bare DNA. While the latter are almost deterministic [11, 12], the former are not. We therefore propose a stochastic model for how the size of a hairpin fluctuates over time. This model includes both the effect of self-avoidance (which tends to shrink the hairpin), and the diffusion caused by thermal motion. Since self-avoidance is relatively weak for our system, the dynamics are dominated by the diffusive term. Our experimental data are in qualitative agreement with the stochastic model. Further experiments and modeling work are necessary to establish a quantitative description of the hairpin fluctuation dynamics.

ACKNOWLEDGMENTS

The labeled RecA protein was a kind gift from Edwige B. Garcin and Mauro Modesti. EW and BM wish to thank Stefano Bo and Tobias Ambjörnsson for discussions concerning Eq. (19). Financial support from Vetenskapsrådet [Grants No. 2013-3992 and 2011-4324] and from the National Institutes of Health (R01-HG006851) is gratefully acknowledged. The computational work was carried out in part using computing resources at the University of Minnesota Supercomputing Institute.

-
- [1] T. Odijk, *Macromolecules* **16**, 1340–1344 (1983).
 - [2] T. W. Burkhardt, Y. Yang, and G. Gompper, *Phys. Rev. E* **82**, 041801 (2010).
 - [3] T. Odijk, *Phys. Rev. E* **77**, 060901 (2008).
 - [4] A. Muralidhar, D. R. Tree, and K. D. Dorfman, *Macromolecules* **47**, 8446 (2014).
 - [5] E. Werner and B. Mehlig, *Phys. Rev. E* **91**, 050601(R) (2015).
 - [6] T. Odijk, *The Journal of chemical physics* **125**, 204904 (2006).
 - [7] B. Nöding and S. Köster, *Phys. Rev. Lett.* **108**, 088101 (2012).
 - [8] W. Reisner, K. Morton, R. Riehn, Y. Wang, Z. Yu, M. Rosen, J. Sturm, S. Chou, E. Frey, and R. Austin, *Phys. Rev. Lett.* **94**, 196101 (2005).
 - [9] W. Reisner, J. N. Pedersen, and R. H. Austin, *Rep. Prog. Phys.* **75**, 106601 (2012).
 - [10] D. R. Tree, Y. Wang, and K. D. Dorfman, *Biomicrofluidics* **7**, 054118 (2013).
 - [11] S. L. Levy, J. T. Mannion, J. Cheng, C. H. Reccius, and H. G. Craighead, *Nano Lett.* **8**, 3839 (2008).
 - [12] M. Alizadehheidari, E. Werner, C. Noble, M. Reiter-Schad, L. K. Nyberg, J. Fritzsche, B. Mehlig, J. O. Tegenfeldt, T. Ambjörnsson, F. Persson, and F. Westerlund, *Macromolecules* **48**, 871 (2015).
 - [13] J. Wang and H. Gao, *J. Chem. Phys.* **123**, 084906 (2005).
 - [14] D. R. Tree, A. Muralidhar, P. S. Doyle, and K. D. Dorfman, *Macromolecules* **46**, 8369 (2013).
 - [15] P. Grassberger, *Phys. Rev. E* **56**, 3682 (1997).
 - [16] T. Prellberg and J. Krawczyk, *Phys. Rev. Lett.* **92**, 120602 (2004).
 - [17] D. R. Tree, Y. Wang, and K. D. Dorfman, *Phys. Rev. Lett.* **110**, 208103 (2013).
 - [18] A. Muralidhar, M. Quevillon, and K. Dorfman, *Polymers* **8**, 79 (2016).
 - [19] K. Frykholm, M. Alizadehheidari, J. Fritzsche, J. Wiggenius, M. Modesti, F. Persson, and F. Westerlund, *Small* **10**, 884 (2014).
 - [20] F. Persson, J. Fritzsche, K. U. Mir, M. Modesti, F. Westerlund, and J. O. Tegenfeldt, *Nano Lett.* **12**, 2260 (2012).
 - [21] “See Supplemental Material at [URL will be inserted by publisher] for a description of our method for computing the global persistence length in simulations and for estimating the relaxation time in experiments, as well as for

kymographic representations of all experiments analysed in this study.”

- [22] J. O. Tegenfeldt, C. Prinz, H. Cao, S. Chou, W. W. Reisner, R. Riehn, Y. M. Wang, E. C. Cox, J. C. Sturm, and P. Silberzan, *Proc. Natl. Acad. Sci. U. S. A.* **101**, 10979 (2004).
- [23] A. Muralidhar and K. D. Dorfman, *Macromolecules* **49**, 1120 (2016).
- [24] M. Hegner, S. B. Smith, and C. Bustamante, *Proc. Natl. Acad. Sci. USA* **96**, 10109 (1999).
- [25] A. Muralidhar and K. D. Dorfman, *Macromolecules* **48**, 2829 (2015).
- [26] G. O. Ibáñez-García, P. Goldstein, and A. Zarzosa-Pérez, *J. Polym. Sci. Part B: Polym. Phys.* **51**, 1411 (2013).
- [27] A. Milchev, L. Klushin, A. Skvortsov, and K. Binder, *Macromolecules* **43**, 6877 (2010).
- [28] E. Werner and B. Mehlig, *Phys. Rev. E* **90**, 062602 (2014).
- [29] M. T. J. van Loenhout, T. van der Heijden, R. Kanaar, C. Wyman, and C. Dekker, *Nucleic Acids Res.* **37**, 4089 (2009).
- [30] A. J. Spakowitz and Z. G. Wang, *J. Chem. Phys.* **119**, 13113 (2003).
- [31] A. Tkachenko and Y. Rabin, *Macromolecules* **28**, 8646 (1995).
- [32] F. Wagner, G. Lattanzi, and E. Frey, *Phys. Rev. E* **75**, 050902 (2007).
- [33] J. Z. Y. Chen, *Macromolecules* **46**, 9837 (2013).

Supplemental material for “Emergence of hairpins in the conformations of a confined polymer”

E. Werner¹, A. Jain², A. Muralidhar², K. Frykholm³, T. St Clere Smithe¹, J. Fritzsche⁴, F. Westerlund³, K. D. Dorfman², B. Mehlig¹

¹*Department of Physics, University of Gothenburg,
Origovägen 6B, 412 96 Göteborg, Sweden*

²*Department of Chemical Engineering and Materials Science,
University of Minnesota – Twin Cities,
421 Washington Avenue SE, Minneapolis, Minnesota 55455, USA*

³*Department of Biology and Biological Engineering,
Chalmers University of Technology,
Kemivägen 10, 412 96 Göteborg, Sweden and*

⁴*Department of Physics, Chalmers University of Technology,
Kemigården 1, 412 96 Göteborg, Sweden*

I. INTRODUCTION

This supplemental material consists of three sections. First, we describe in detail how the global persistence length was computed in simulations. Second, we show the autocorrelation functions for molecules that are free of hairpins, and discuss how the relaxation time was estimated from the autocorrelation. Finally, we show a visual representation of all the experimental videos that were analyzed in this study, in the form of kymographs.

II. CALCULATION OF GLOBAL PERSISTENCE LENGTH

We calculated the global persistence length by using the simulation data for the mean-square extension of the chain projected along the channel axis, $\langle R_x^2 \rangle$, and fitting them to [1, 2]

$$\langle R_x^2 \rangle = \frac{1}{3}(1 + 2m)[2gL - 2g^2(1 - \exp(-L/g))] \quad (\text{S1})$$

where

$$m = \frac{1}{2}(3\langle \cos^2 \theta \rangle - 1) \quad (\text{S2})$$

is the orientational order parameter [1, 3, 4], and θ is the angle formed between the tangent to the chain backbone and the channel axis. We used 10^6 tours for $D_W = 3 \mu\text{m}$, 5×10^5 tours for $D_W = 2.4 \mu\text{m}$, 2.5×10^5 tours for $D_W = 1.8 \mu\text{m}$, 2×10^4 tours for $D_W = 1.3 \mu\text{m}$, and 5×10^4 tours for $D_W = 0.9 \mu\text{m}$. The simulations used ideal chains with 10^5 beads. The results were unaffected by increasing the number of beads. For $D_W = 0.9 \mu\text{m}$ and $1.3 \mu\text{m}$, we set the bead size to 20 nm in order to obtain a sufficiently large contour length; all other simulations used bead sizes of 10 nm.

We determined g by minimizing the mean-square error between the simulation data and Eq. (S1) with respect to g . This provided us the optimum values of g for each D_W . Note that we ran PERM simulations for $N_b = 100,000$ beads for these calculations. Plots of the mean-square error as a function of the fitting parameter g are shown in Fig. S1. For the smallest channel no minimum was found, indicating that for these parameters the global persistence length is much larger than the our maximal contour length. Therefore, we do not have the value of g for $D_W = 600 \text{ nm}$. Finally, Fig. S2 shows the simulation data (dashed lines) along with the fitted data (solid lines) for all channel sizes.

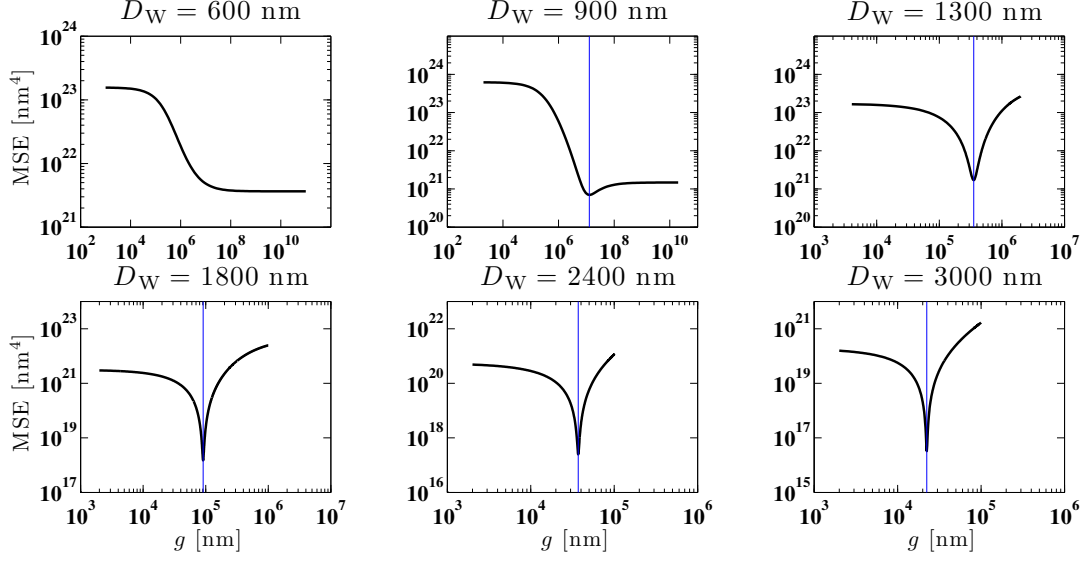


FIG. S1. The mean-square error (MSE) between the simulation data for $\langle R_x^2 \rangle$ and Eq. (S1), as a function of the fitting parameter g , for all channel sizes. The blue vertical lines indicate the minima and hence the optimal values of g .

We calculated the global persistence length for one more case, i.e., for $\ell_P = 1150$ nm and $D_W = 600$ nm. We performed simulations for this parameter set to allow us to obtain ℓ_{SA} and hence α with better statistics (see Fig. 2 of the main text). Fig. S3 shows the mean-square error as a function of the fitting parameter g , and Fig. S4 shows the simulation data for $\langle R_x^2 \rangle$ (dashed line) along with the fitted data (solid line).

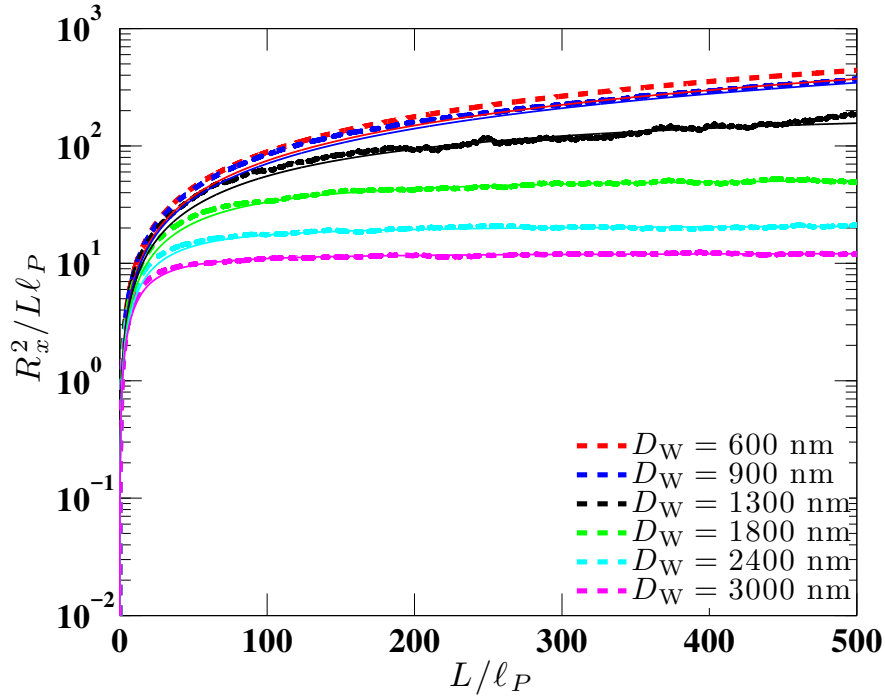


FIG. S2. Mean-square extension of the chain projected along the channel axis, as a function of the contour length L , for all values of D_W considered in this work. The dashed lines indicate simulation data which are fitted using Eq. (S1) in the manuscript. The fitted lines are shown using corresponding solid lines. The value of ℓ_P is 2000 nm.

III. THE RELAXATION TIME WITHOUT HAIRPINS

To measure the relaxation time for the subset of molecules that are free of hairpins we first removed all videos showing hairpins by manual inspection. Next, we plotted the extension as a function of time and removed a small number of time series showing unexpected behavior, usually a strong drift (indicating that the molecule was not in equilibrium at the start of the measurement). We then measured the autocorrelation function

$$C(\tau) = \frac{\langle [X(t) - \langle X \rangle][X(t + \tau) - \langle X \rangle] \rangle}{\langle [X(t) - \langle X \rangle]^2 \rangle}. \quad (\text{S3})$$

Fig. S5 shows this autocorrelation function for each individual video. Fig. S5 also shows the average autocorrelation function over all molecules, as well as the standard deviation of $C(\tau)$ over different molecules. From the autocorrelation function, the relaxation time was estimated by two different methods. First, we integrated the average correlation function

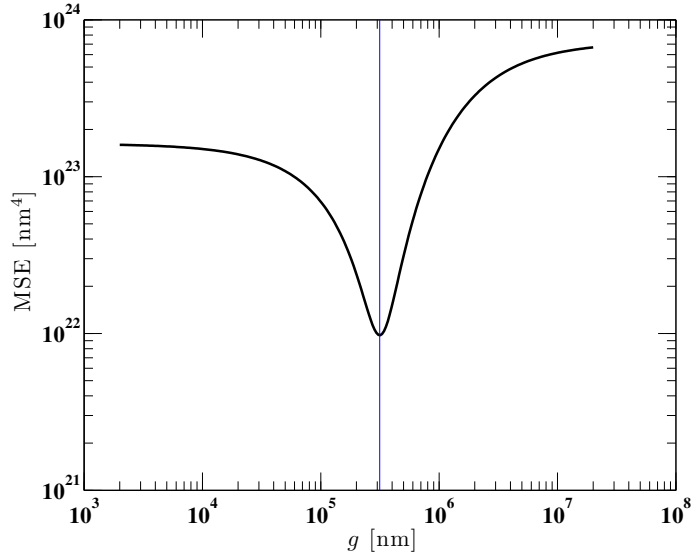


FIG. S3. The mean-square error (MSE) between the simulation data for $\langle R_x^2 \rangle$ and Eq. (S1), as a function of the fitting parameter g , for $\ell_P = 1150$ nm and $D_W = 600$ nm. The blue vertical line indicates the minimum and hence the optimal value of $g = 314.9$ μm .

up to a cutoff at 20 frames (2.2 s), yielding

$$\tau_{\text{relax}} = \int_0^{2.2 \text{ s}} d\tau C(\tau). \quad (\text{S4})$$

Second, we obtained an estimate by assuming that the initial correlation function decays as an exponential function,

$$\log C(\tau) = A + B\tau. \quad (\text{S5})$$

The parameter $\tau_{\text{relax}} = -1/B$ was then obtained by a least squares fit of the above equation (with free parameters A and B) against the first 4 frames of $C(\tau)$, i.e. between 0 and 0.44 s. These estimates are plotted in Fig. 6 of the main article, together with an estimate of the variability that was computed by replacing the average correlation function in Eqs. (S4)–(S5) by the upper and lower standard deviation, i.e. the functions given by the upper and lower boundary of the gray region in Fig. S5.

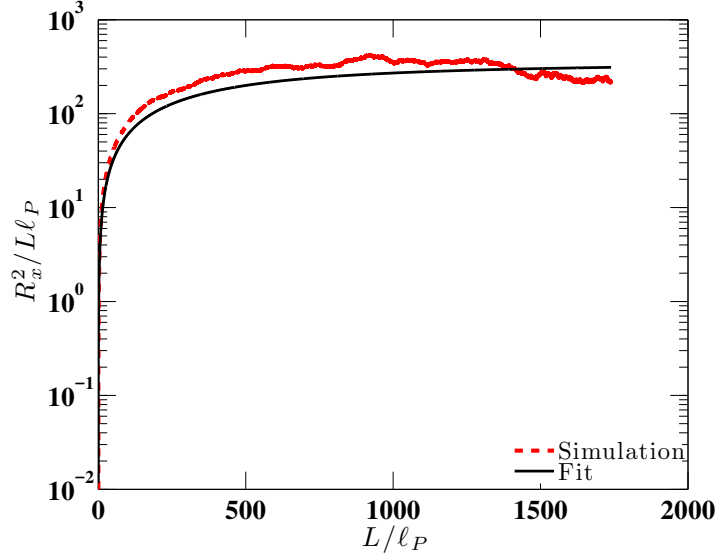


FIG. S4. Mean square extension of the chain projected along the channel axis, as a function of the contour length L , for $\ell_P = 1150$ nm and $D_W = 600$ nm. The dashed red line indicates simulation data which are fitted using Eq. (S1) in the manuscript. The fitted line is shown by the solid line.

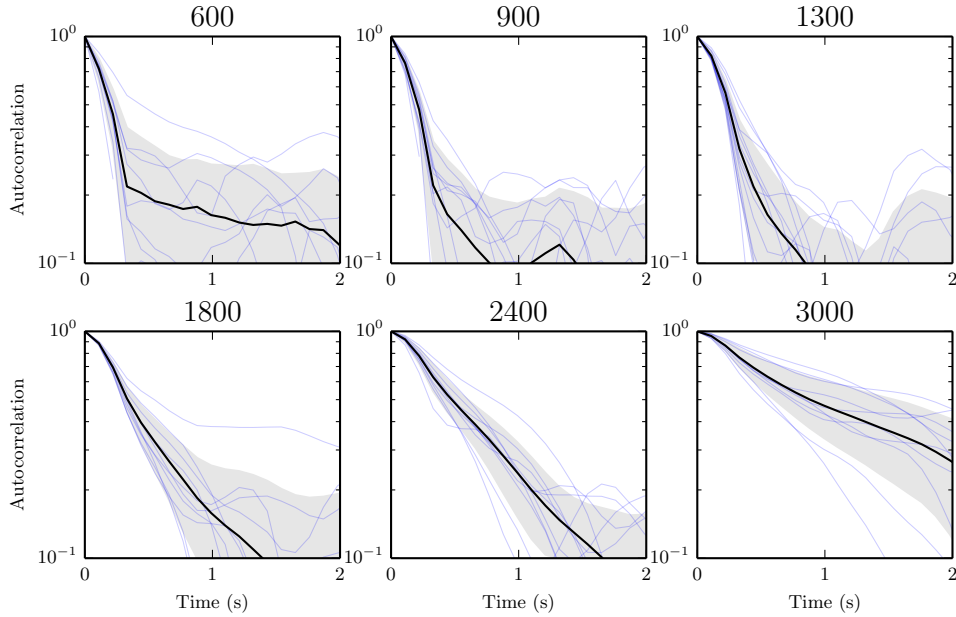


FIG. S5. Autocorrelation functions in different channels, for polymers without hairpins and $12 \mu m < L < 18 \mu m$. Light-blue curves: Autocorrelation functions for individual molecules. Black curve: The average over all individual autocorrelation functions. The gray region denotes one standard deviation above and below the average autocorrelation.

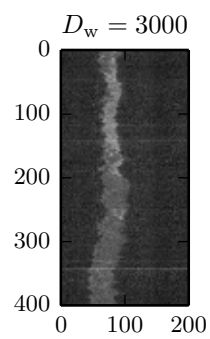
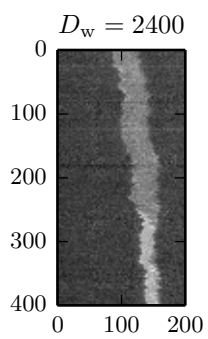
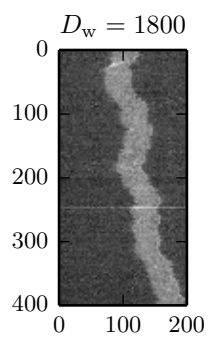
IV. LIST OF KYMOGRAPHS

The kymographs (see section II C of the main text) of all recorded molecules are listed below. Note that not all molecules have been recorded in all channels. The molecule identifier includes the following information (from left to right):

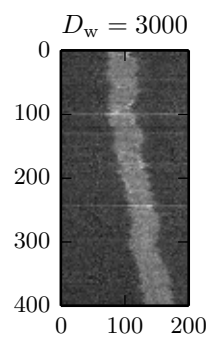
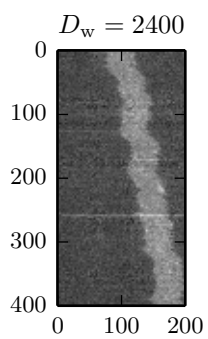
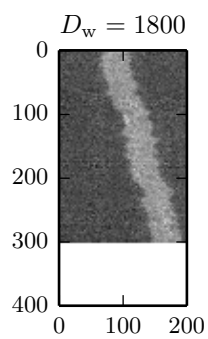
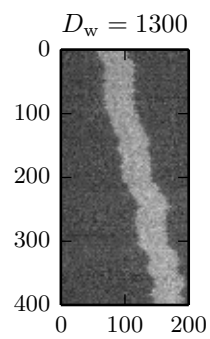
1. Acquisition date.
2. Polymer type, either RecA-T4 or RecA-lambda.
3. The order in which the molecule traversed the different channels. ‘wide’ indicates that the videos were recorded in order of decreasing channel size, ‘narrow’ that the videos were recorded in order of increasing channel size.
4. A single number to uniquely identify each molecule.

-
- [1] A. J. Spakowitz and Z. G. Wang, *J. Chem. Phys.* **119**, 13113 (2003).
[2] A. Tkachenko and Y. Rabin, *Macromolecules* **28**, 8646 (1995).
[3] F. Wagner, G. Lattanzi, and E. Frey, *Phys. Rev. E* **75**, 050902 (2007).
[4] J. Z. Y. Chen, *Macromolecules* **46**, 9837 (2013).

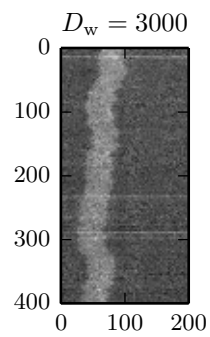
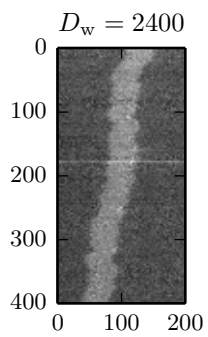
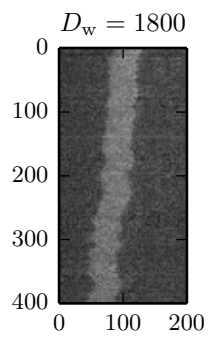
130603-RecA-T4-wide-2



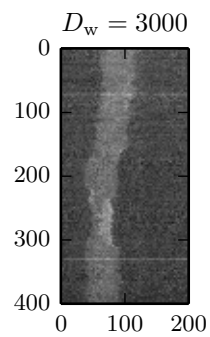
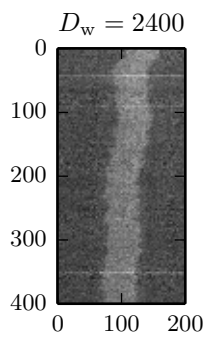
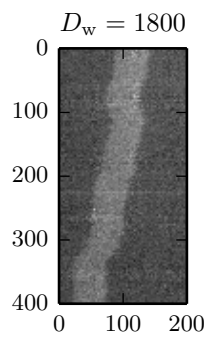
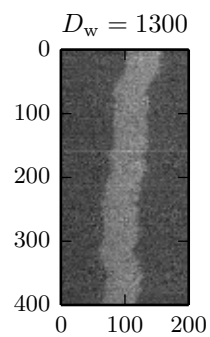
130603-RecA-T4-wide-3



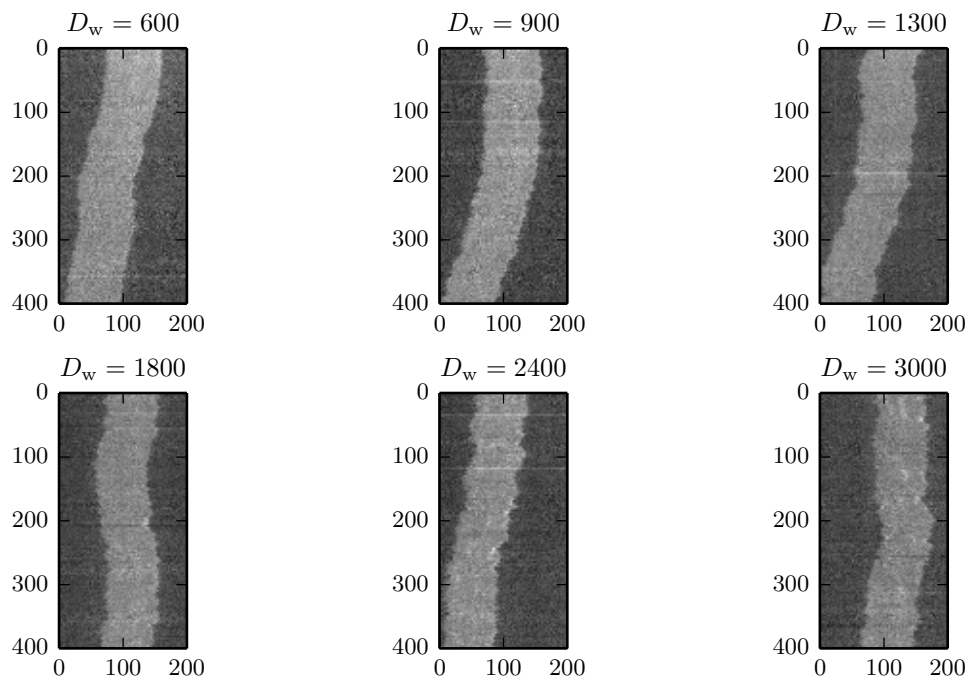
130603-RecA-T4-wide-4



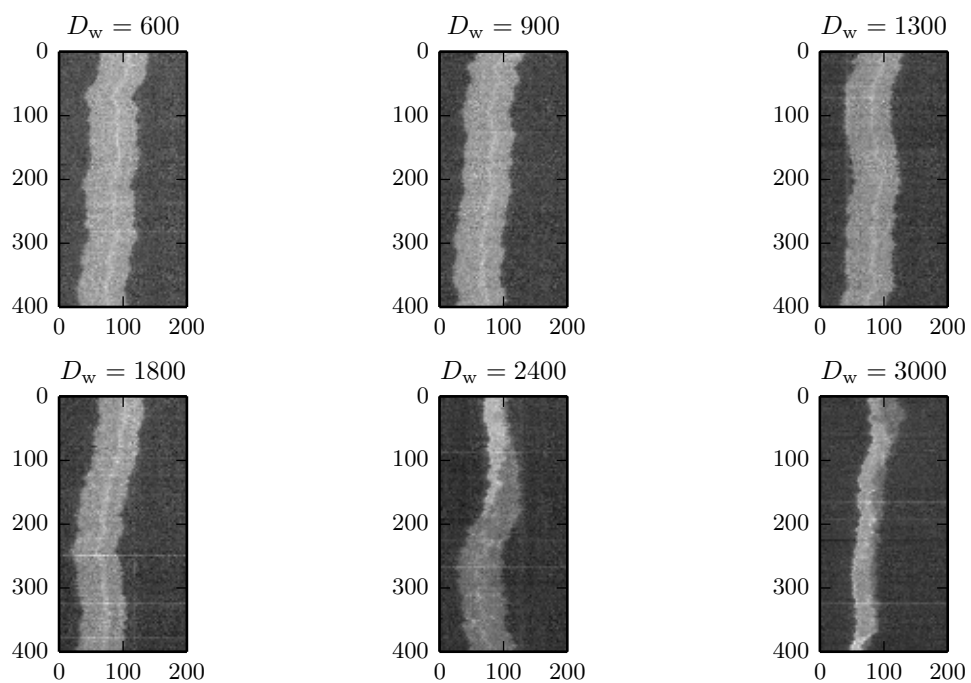
130603-RecA-T4-wide-5



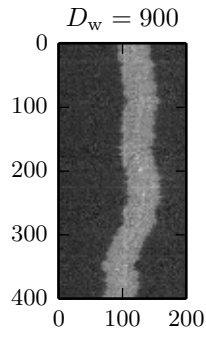
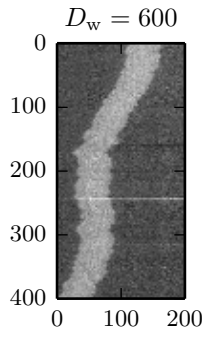
130603-RecA-T4-wide-7



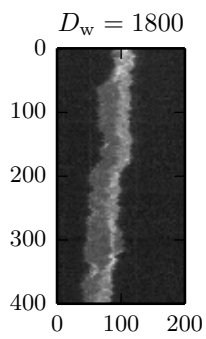
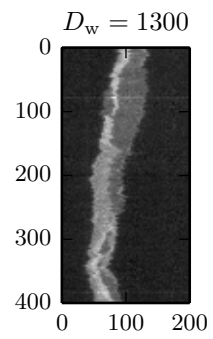
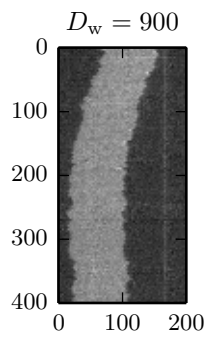
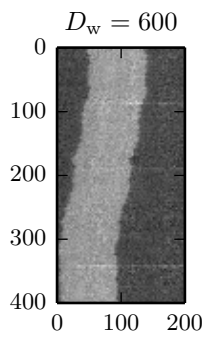
130607-RecA-T4-narrow-10



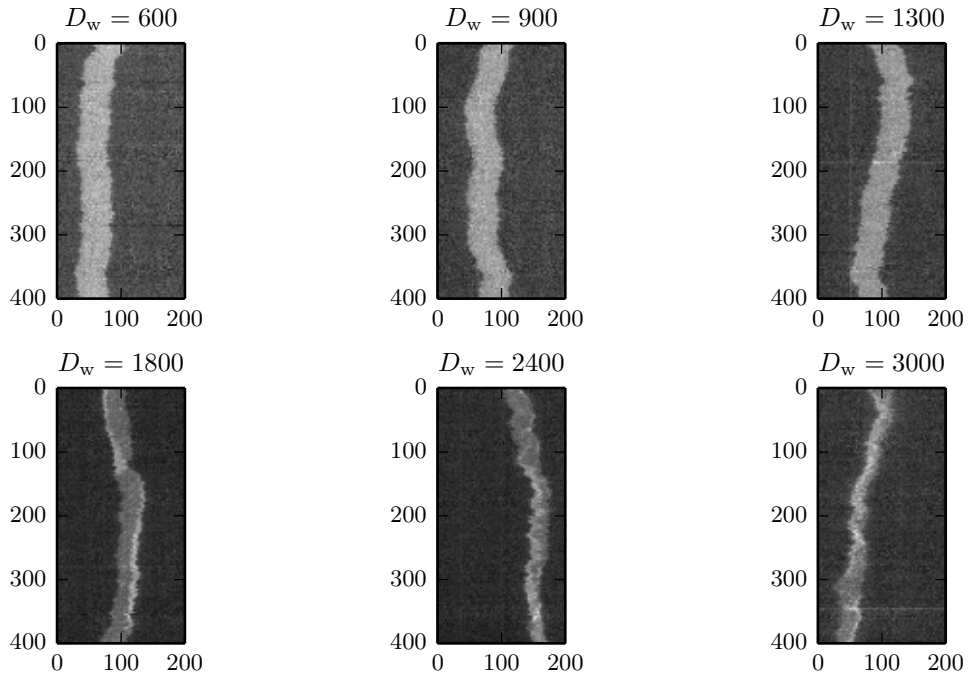
130607-RecA-T4-narrow-7



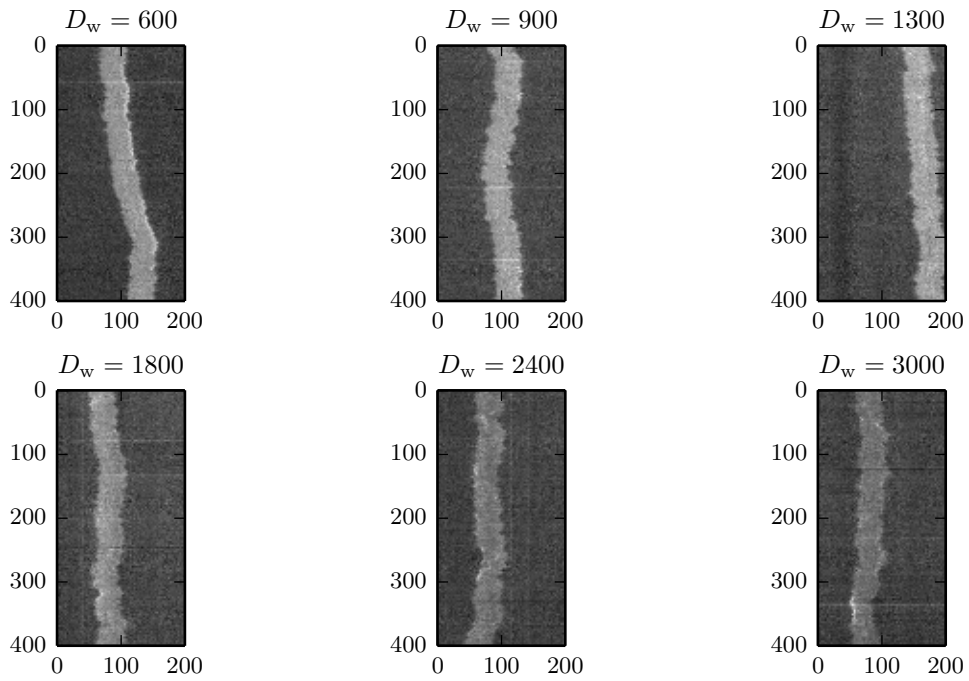
130607-RecA-T4-narrow-8



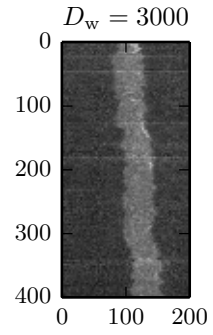
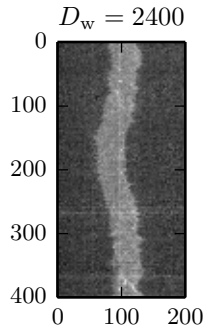
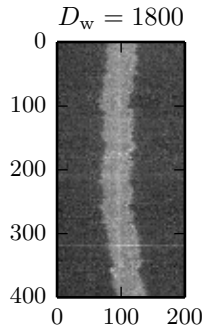
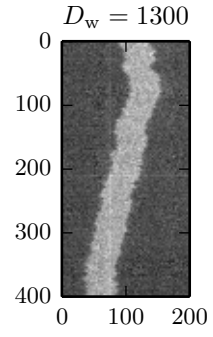
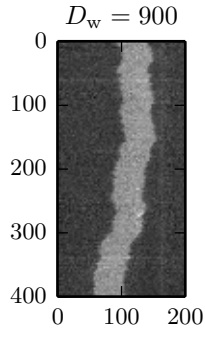
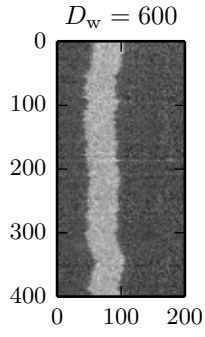
130607-RecA-T4-narrow-9



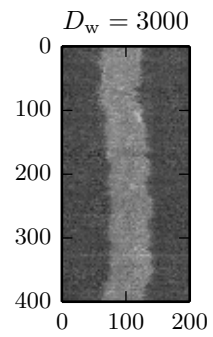
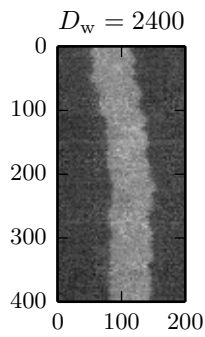
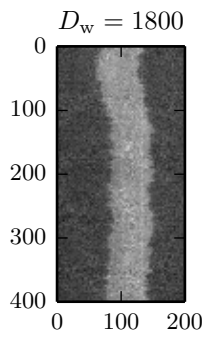
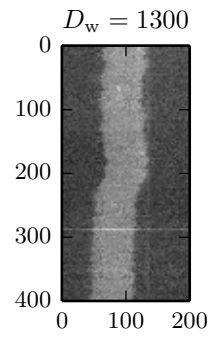
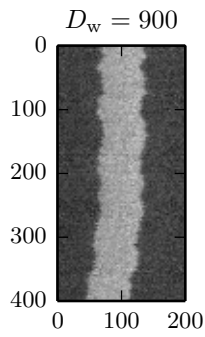
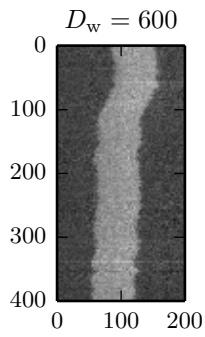
130607-RecA-T4-wide-1



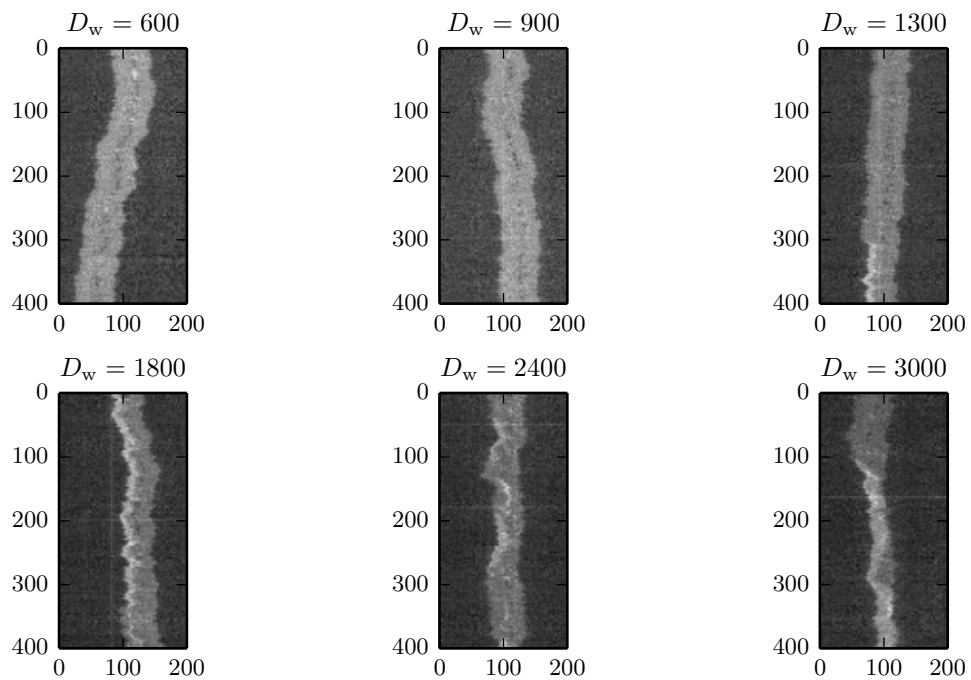
130607-RecA-T4-wide-2



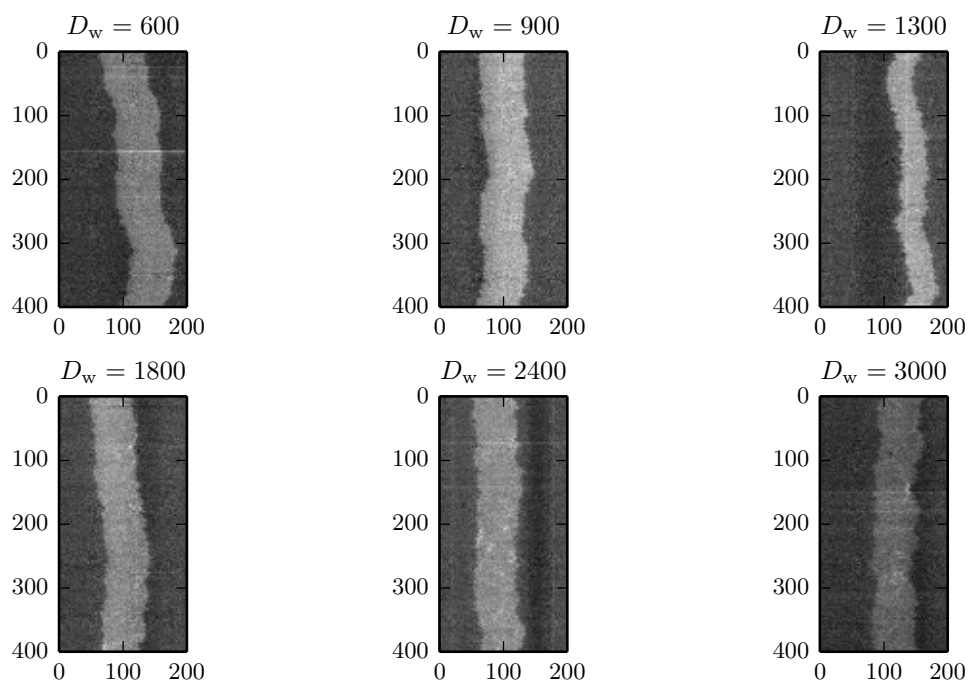
130607-RecA-T4-wide-3



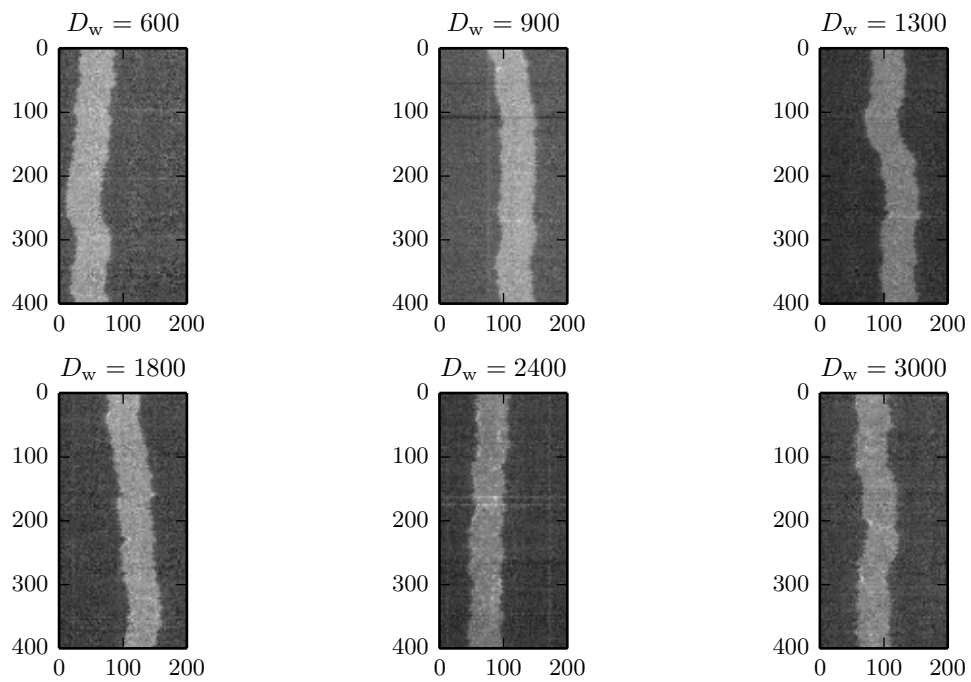
130607-RecA-T4-wide-4



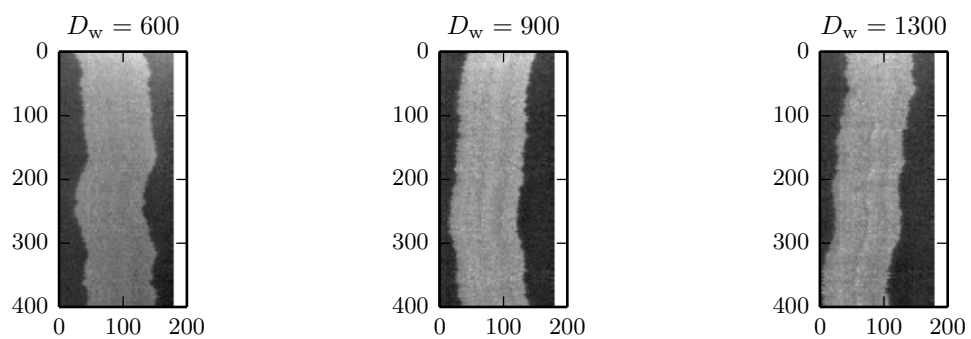
130607-RecA-T4-wide-5



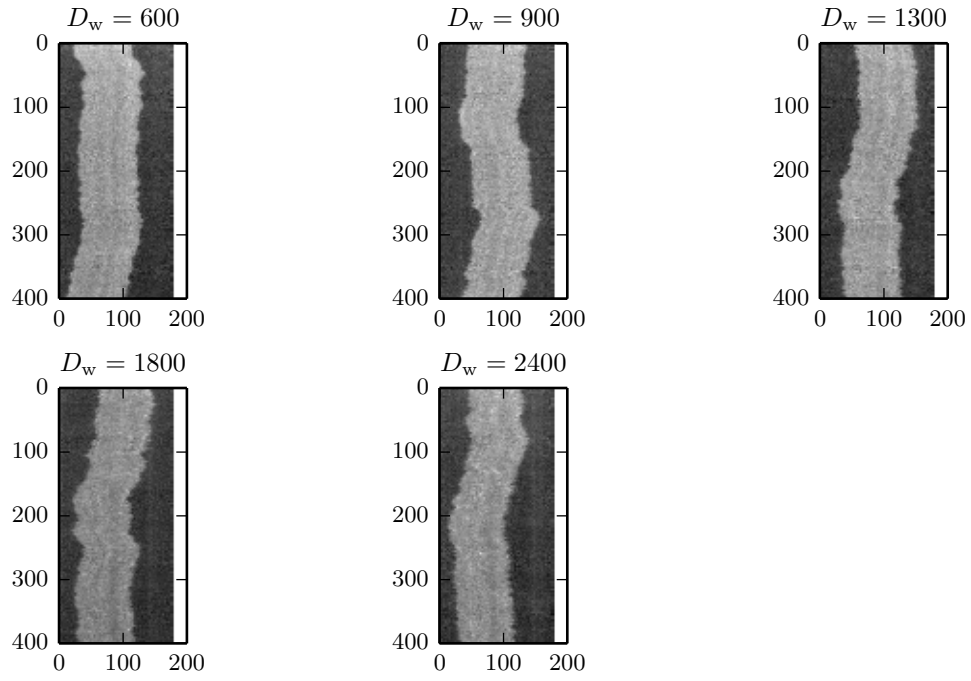
130607-RecA-T4-wide-6



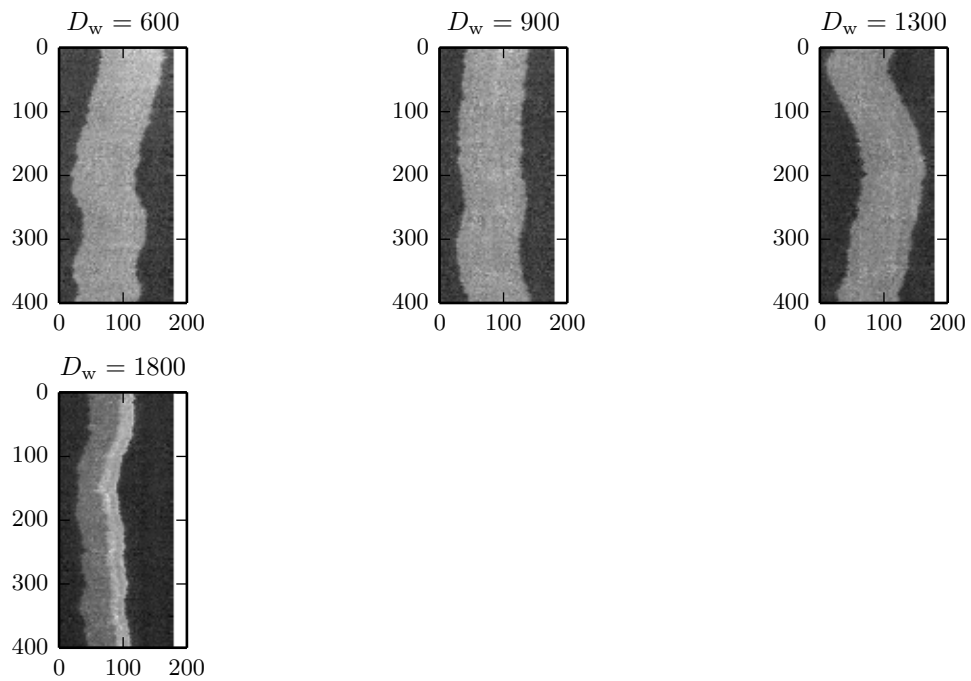
130905-RecA-T4-narrow-1



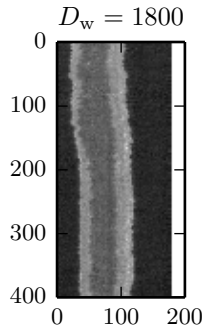
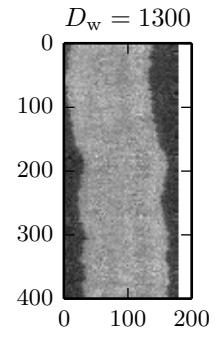
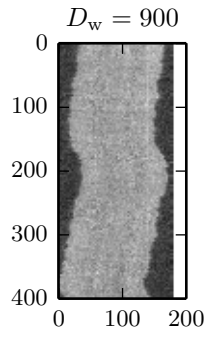
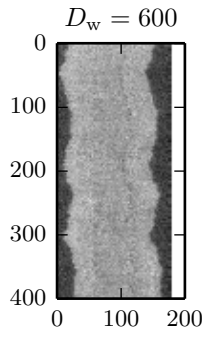
130905-RecA-T4-narrow-2



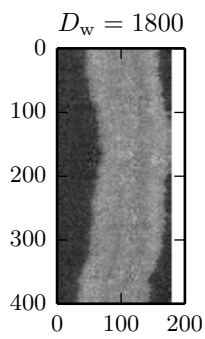
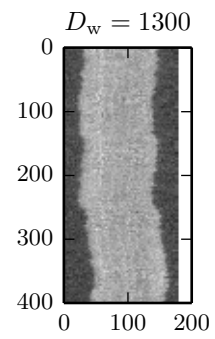
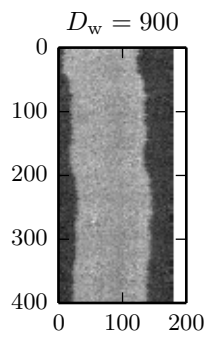
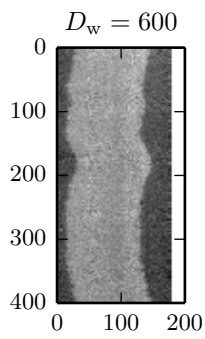
130905-RecA-T4-narrow-3



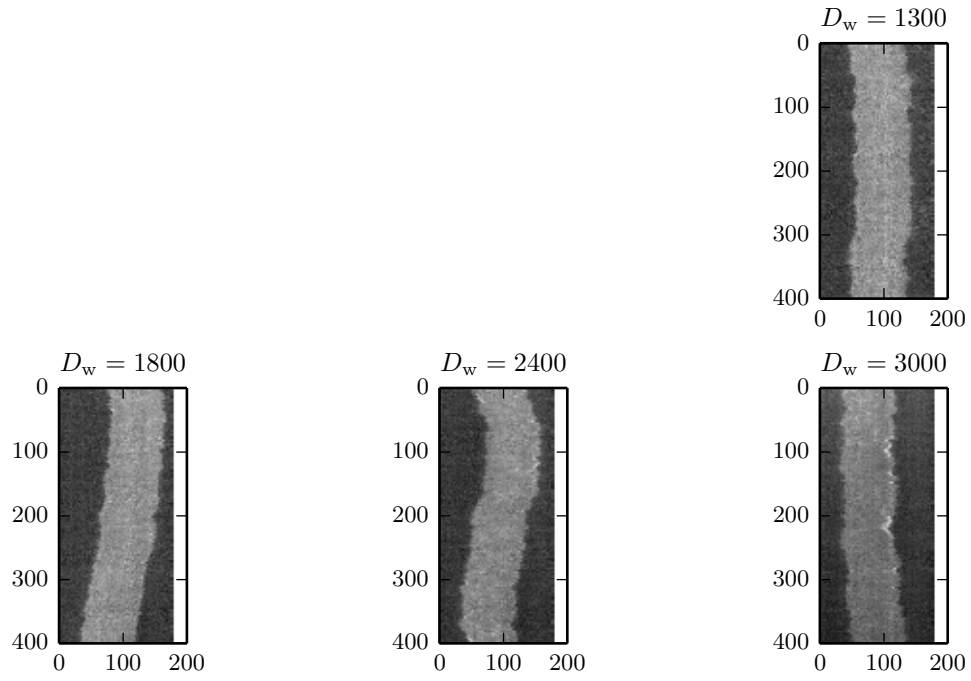
130905-RecA-T4-narrow-4



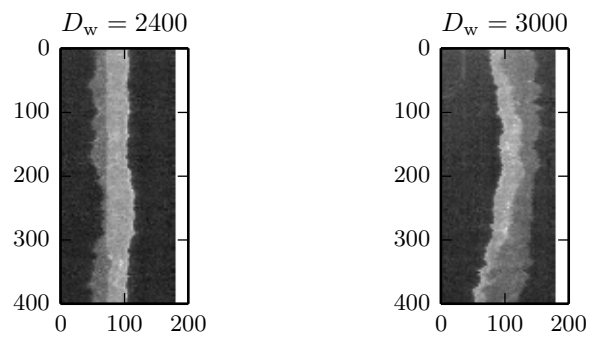
130905-RecA-T4-narrow-5



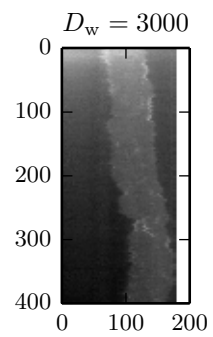
130905-RecA-T4-narrow-6



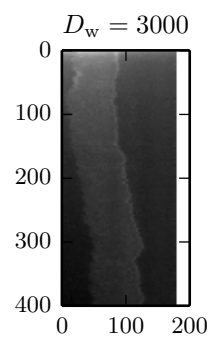
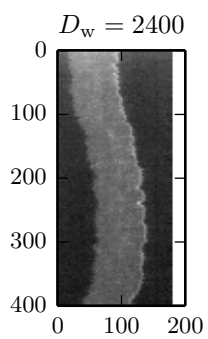
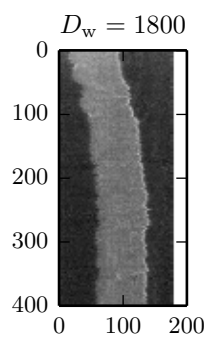
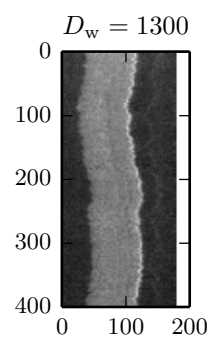
130905-RecA-T4-narrow-7



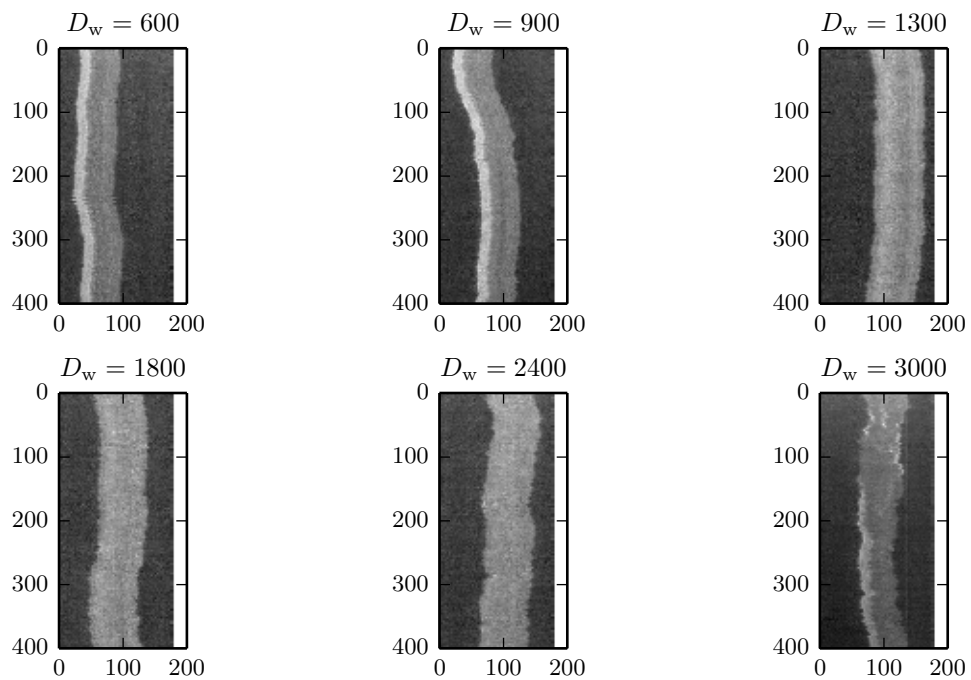
130905-RecA-T4-wide-1



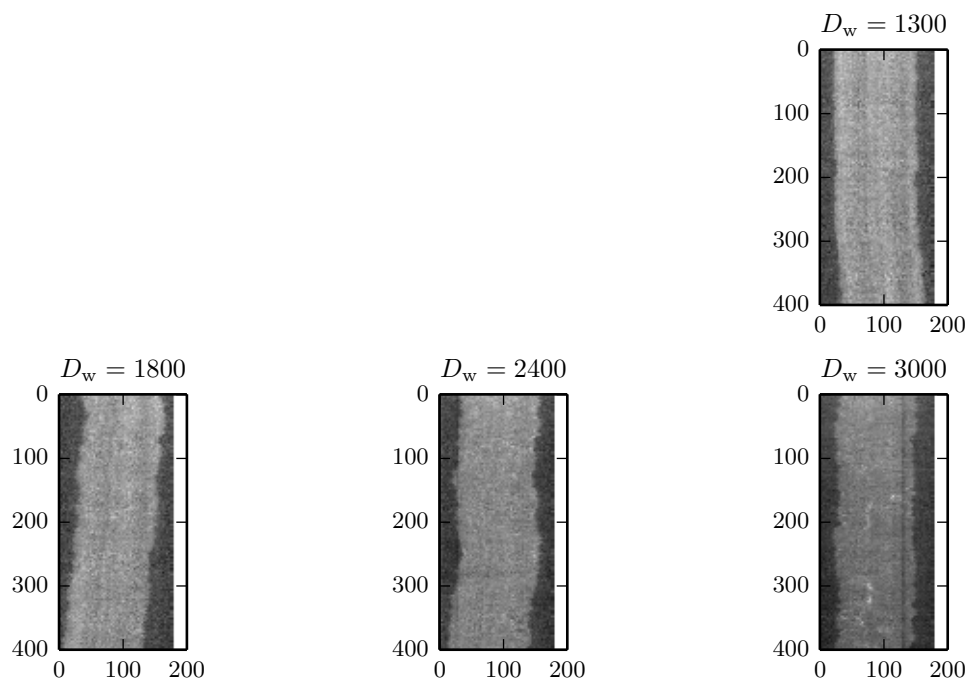
130905-RecA-T4-wide-2



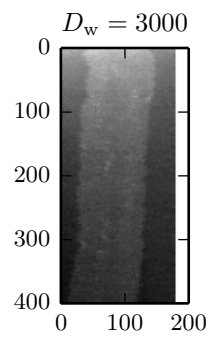
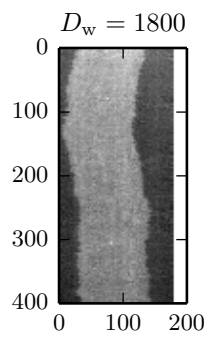
130905-RecA-T4-wide-3



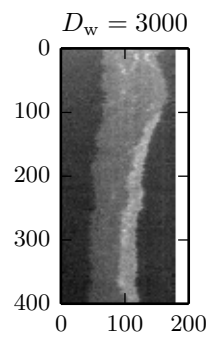
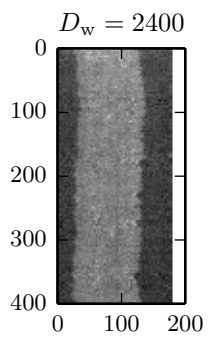
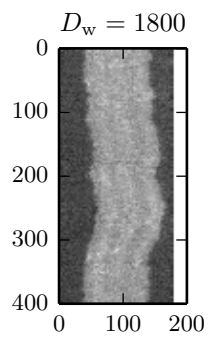
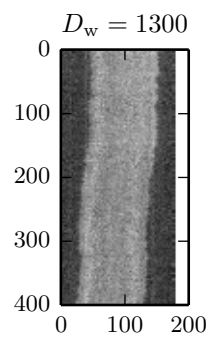
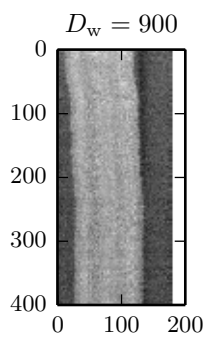
130905-RecA-T4-wide-4



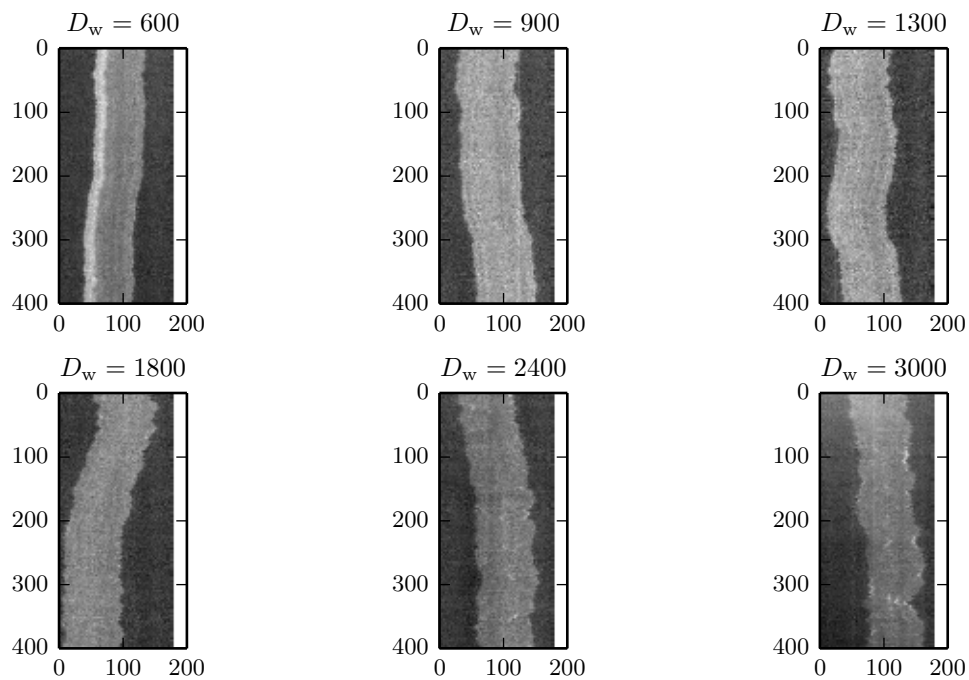
130905-RecA-T4-wide-5



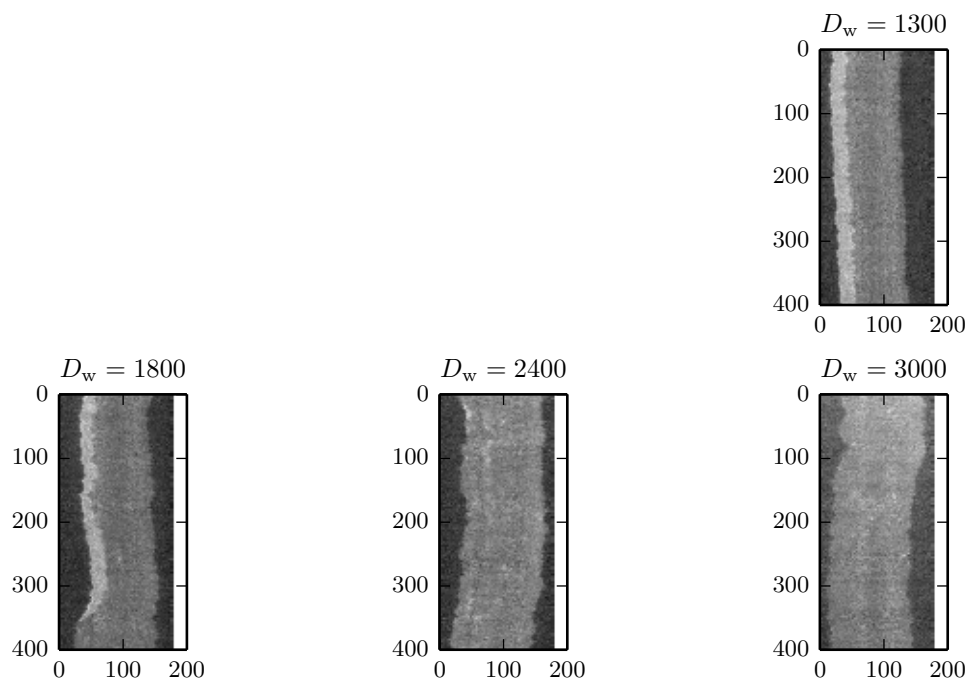
130905-RecA-T4-wide-6



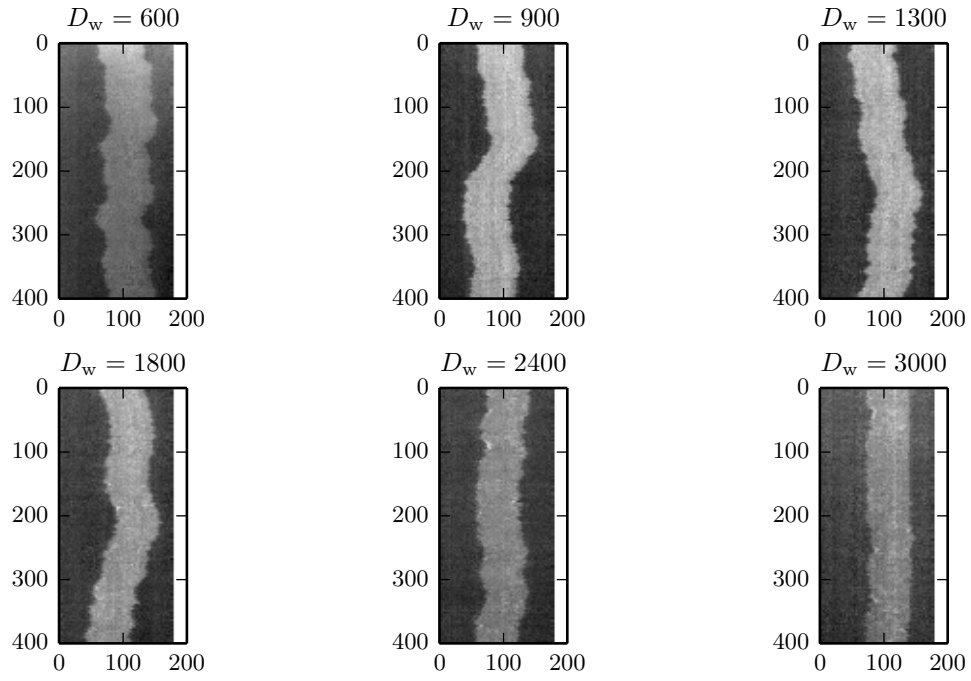
130905-RecA-T4-wide-7



130905-RecA-T4-wide-8



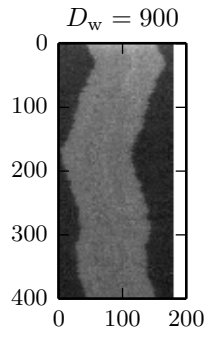
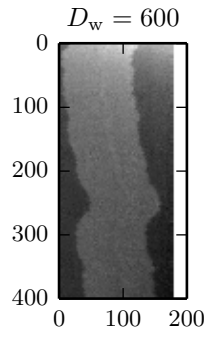
130924-RecA-lambda-narrow-1



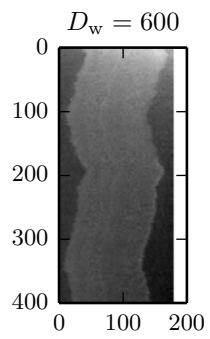
130924-RecA-lambda-narrow-2



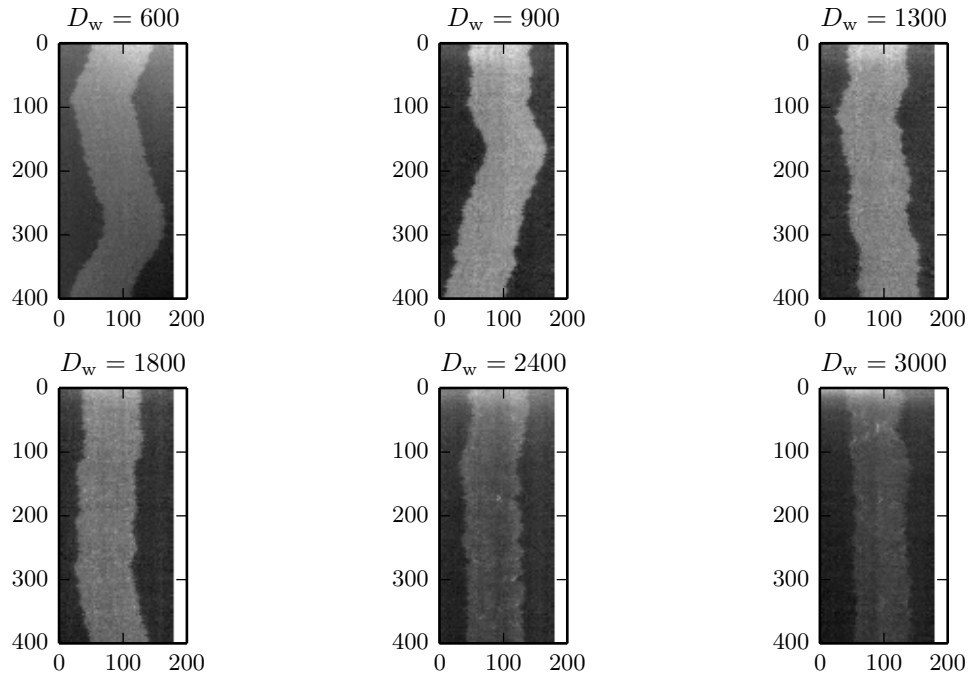
130924-RecA-lambda-narrow-3



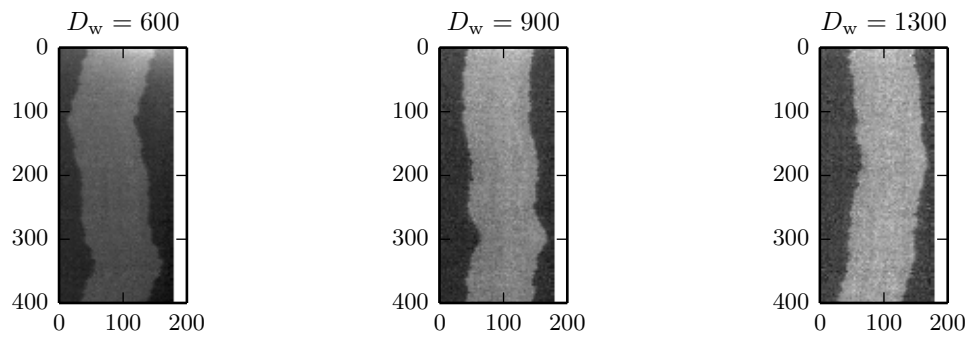
130924-RecA-lambda-narrow-4



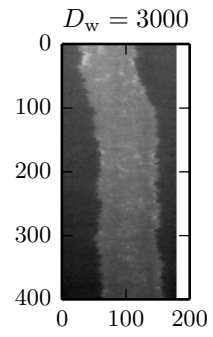
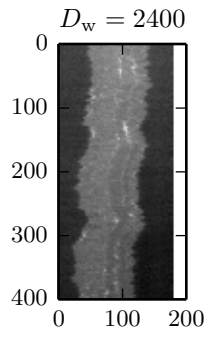
130924-RecA-lambda-narrow-5



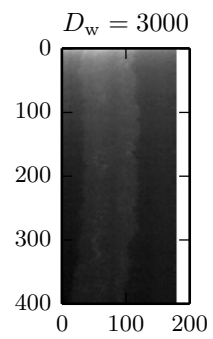
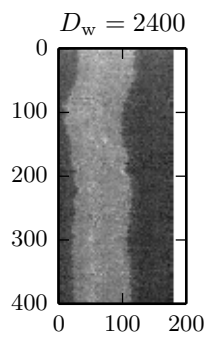
130924-RecA-lambda-narrow-6



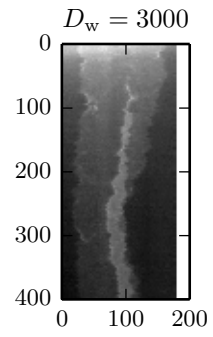
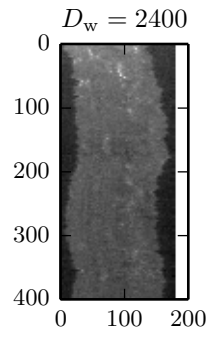
130924-RecA-lambda-wide-1



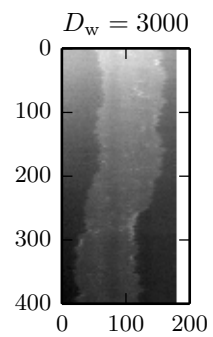
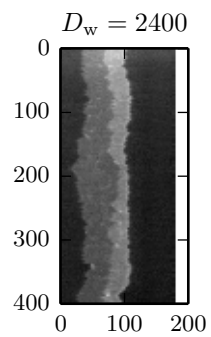
130924-RecA-lambda-wide-10



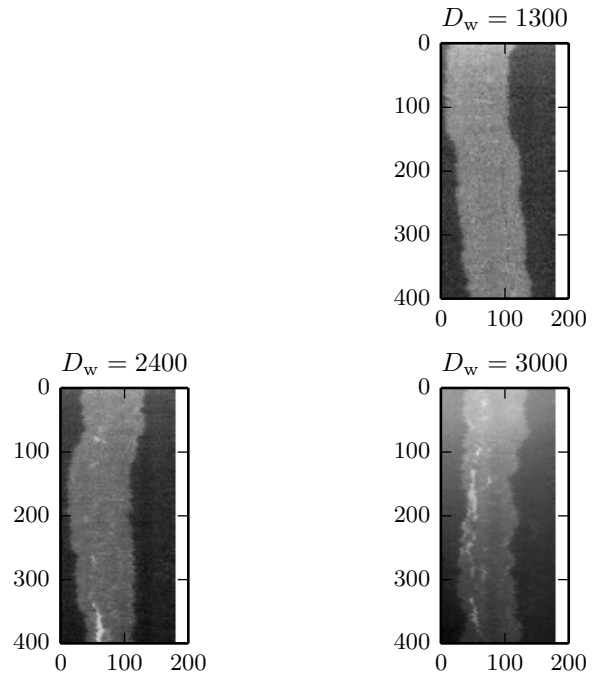
130924-RecA-lambda-wide-2



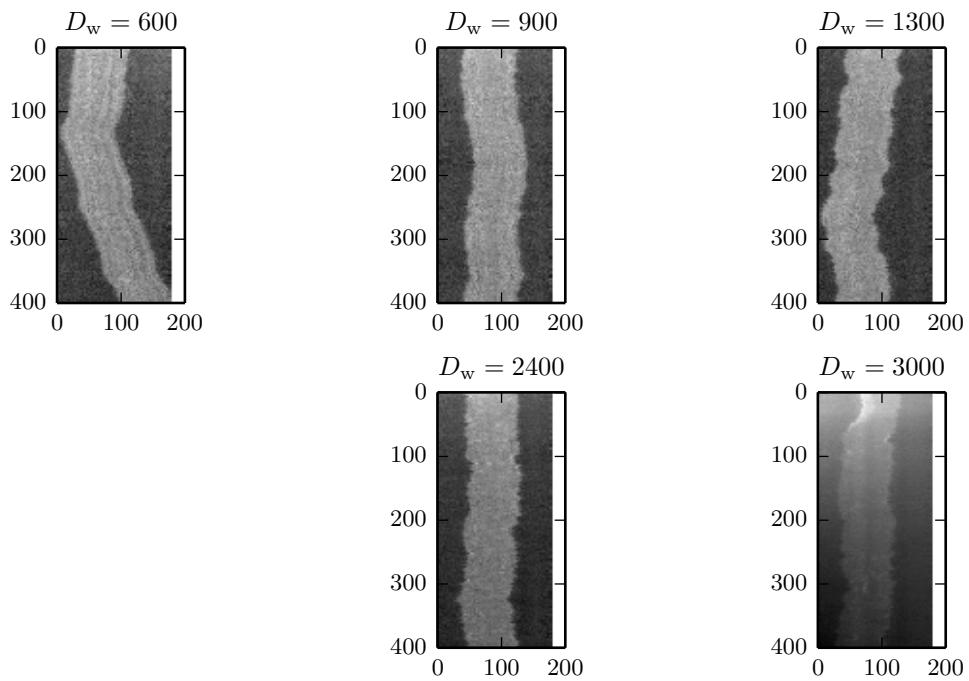
130924-RecA-lambda-wide-3



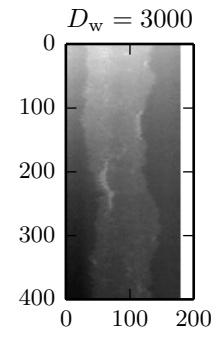
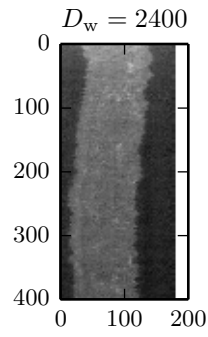
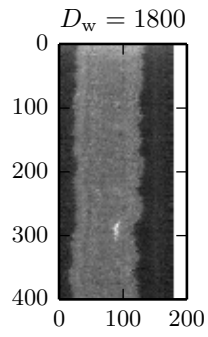
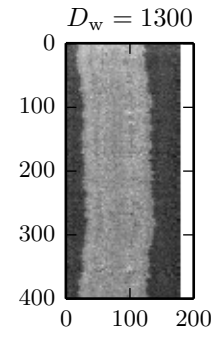
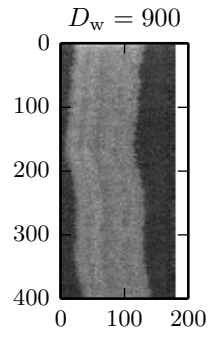
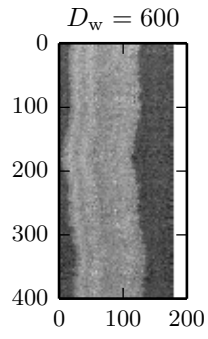
130924-RecA-lambda-wide-4



130924-RecA-lambda-wide-5



130924-RecA-lambda-wide-8



130924-RecA-lambda-wide-9

